Applied Physics Reviews

REVIEW ARTICLE | MARCH 10 2025

Defect-induced magnetic symmetry breaking in oxide materials

Eric Brand ; Victor Rosendal ; Yichen Wu ; Thomas Tran ; Alessandro Palliotto ;
Igor V. Maznichenko ; Sergey Ostanin ; Vincenzo Esposito ; Arthur Ernst ; Shengqiang Zhou ;
Dae-Sung Park ✉ ; Nini Pryds ✉

Appl. Phys. Rev. 12, 011327 (2025)
https://doi.org/10.1063/5.0216796

AIP Publishing

Applied Physics Reviews REVIEW pubs.aip.org/aip/are

Defect-induced magnetic symmetry breaking in oxide materials

Cite as: Appl. Phys. Rev. **12**, 011327 (2025); doi: 10.1063/5.0216796
Submitted: 1 May 2024 · Accepted: 11 February 2025 ·
Published Online: 10 March 2025

Eric Brand,[1] Victor Rosendal,[1] Yichen Wu,[1] Thomas Tran,[1] Alessandro Palliotto,[1] Igor V. Maznichenko,[2,3,4] Sergey Ostanin,[2] Vincenzo Esposito,[1] Arthur Ernst,[4,5] Shengqiang Zhou,[6] Dae-Sung Park,[1,a)] and Nini Pryds[1,a)]

AFFILIATIONS

[1] Department of Energy Conversion and Storage, Technical University of Denmark, Kongens, Lyngby 2800, Denmark
[2] Institut für Physik, Martin-Luther-Universität Halle-Wittenberg, 06099 Halle, Germany
[3] Department of Engineering and Computer Sciences, Hamburg University of Applied Sciences, Berliner Tor 7, D-20099 Hamburg, Germany
[4] Max Planck Institute of Microstructure Physics, 06120 Halle, Germany
[5] Institute of Theoretical Physics, Johannes Kepler University, 4040 Linz, Austria
[6] Helmholtz-Zentrum Dresden-Rossendorf, Institute of Ion Beam Physics and Materials Research, Bautzner Landstraße 400, 01328 Dresden, Germany

[a)] Authors to whom correspondence should be addressed: nipr@dtu.dk and daepa@dtu.dk

ABSTRACT

Magnetic properties of crystalline solids are fundamental to a wide range of applications, capturing the attention of a vast scientific community. Thus, engineering magnetic order in materials such as ferromagnetism and antiferromagnetism holds great scientific and technological interest. Defects such as vacancies, interstitials, and dopants induce local perturbations within the crystal lattice. These perturbations locally disturb the entire symmetry of crystals, resulting in symmetry breaking. Oxides, in particular, exhibit intriguing properties when subjected to defects, which can lead to significant modifications in their structural, electronic, and magnetic properties. Such defects in non-magnetic oxides can induce magnetic symmetry breaking, leading to the formation of emergent magnetic domains and orderings. In this review, we focus on the recent progress in magnetic breaking symmetries in materials via defect engineering and present our perspectives on how these may lead to new understanding and applications.

TABLE OF CONTENTS

I. INTRODUCTION

In condensed matter physics, the magnetism of crystalline oxide materials has long been a captivating endeavor, unraveling mesmerizing magnetic phenomena with unprecedented combination of spin arrangements and crystal symmetries. Traditionally, the study of magnetism in oxides has centered on ordered crystal structures and predictable magnetic behaviors arising from well-defined atomic arrangements. However, a new and intriguing frontier has emerged in recent years, challenging the conventional wisdom—"*Defect-induced magnetism.*"[1–3]

Control over the functional property of oxide film materials can be obtained by modulating two parts: epitaxial strain and defects.[4,5] Epitaxy and strain generation, originating from the lattice mismatch between thin films and single-crystal substrates, can be partially or fully released at the interface between the epitaxial film and substrates via the formation of edge dislocations that periodically distribute along the interface. This is the most widely used tool to tune material structures and properties in oxide thin films. The second significant aspect of modulating oxide properties is via defect management: the careful balance of atomic defects and their orderings.[6–8] Point defects represent a deviation from the long-range periodicity of the crystal lattice. The key types of point defects include vacancies (e.g., oxygen vacancies, V_O and cation vacancies, V_C), interstitials, and anti-site defects.[7,9] Oxygen vacancy is one of the most common defects in metal oxides and, in many cases, determines the properties of the oxides.[10,11] Therefore, accurate control over the oxygen vacancy concentration and distribution is desired.

Magnetic order at room temperature induced by atomic lattice defects, such as vacancies and interstitials, has been observed in many oxides and is crucial for technological applications. Magnetic order refers to the alignment of magnetic moments of atoms or ions in a specific pattern, leading to the emergence of macroscopic magnetism and is rooted in the magnetic moments' mechanisms, which are associated with the intrinsic spin and orbital angular momentum of electrons in atoms.[12,13] Point defects like vacancies can significantly alter electron orbits, potentially creating large local magnetic moments. The defect-induced magnetism in oxides is based on precise control of defects and is crucial for tailoring their magnetic properties.[14] However, creating and manipulating such defects in materials at the atomic level with a homogeneous distribution at specific lattice positions remains challenging since the defects are often sensitive to processing conditions and reactivity toward the environment, e.g., at the surface. Therefore, ensuring high sample purity and avoiding unintended defect generation during synthesis or processing are crucial for accurately controlling the defect concentration.

One of the primary challenges is to fully describe and understand the mechanisms by which defects influence magnetism in oxide materials.[6,15] Defects can introduce localized magnetic moments or alter the spin configuration in the material, but the exact processes and interactions involved can be complex and challenging to interpret. Developing comprehensive theoretical models that accurately describe these interactions and defects at the atomic scale remains a significant challenge. Despite these challenges, researchers are continually progressing in understanding and manipulating defect-induced magnetism in oxide materials, some of which will be discussed in this review paper, see Fig. 1.

The primary objective of this review paper is to provide comprehensive insights into the current realm of defect-induced magnetism. The intriguing symmetry-breaking phenomenon is at the heart of interfacial magnetism. Turning to extended defects, an exciting model system is the planar interfaces, e.g., $LaAlO_3/SrTiO_3$ and spinel γ-$Al_2O_3/SrTiO_3$ heterostructures.[6,15] Another aim is to explore how interfaces give rise to exchange bias, where the magnetic moments of one material become pinned or aligned by the adjacent antiferromagnetic or spin-glass material. By examining the theoretical models, experimental findings, and emerging research trends, we aim to

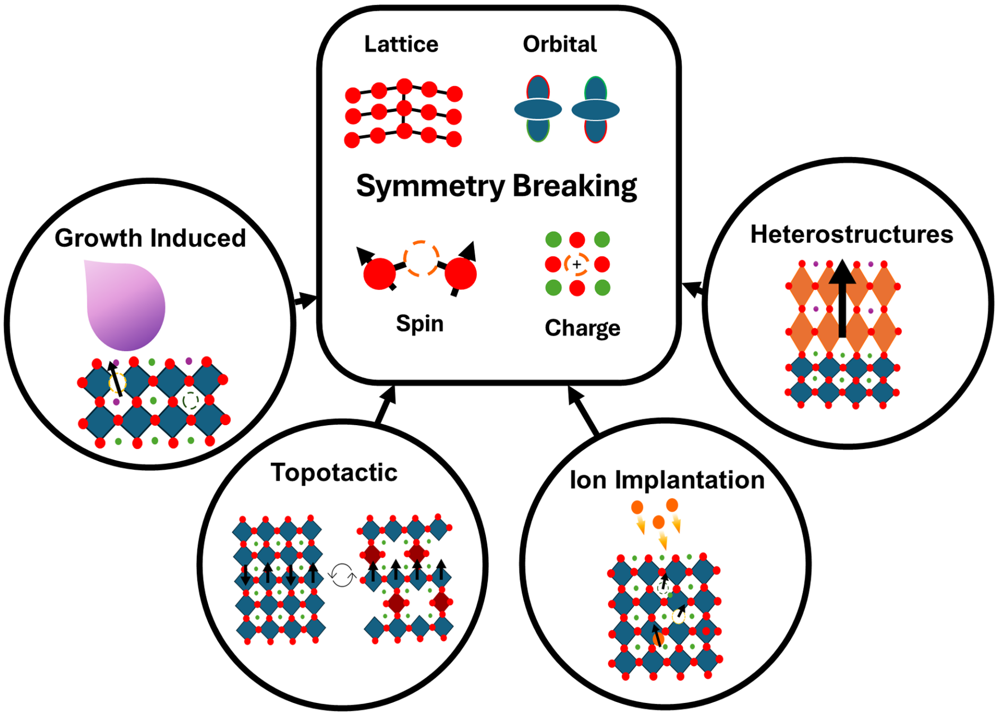

FIG. 1. The defect induced magnetism through lattice, orbital, spin, and charge symmetry breaking. It also highlights strategies for engineering these defects, including growth-induced defects, heterostructural strain and interfaces, topotactic phase transitions, and ion implantation-induced interstitials and point defects.

elucidate the crucial influence of defects and symmetry breaking on the magnetic behavior in solid oxide materials.

This review paper is structured in the following way: Sec. II provides a concise overview of emergent magnetism associated with point defects (V_O and V_C) and the effect of oxide thin film growth conditions, tunable magnetism by defect-mediated crystal structure distortion and dopants, and magnetism arising from extended structure defects. In Sec. III, we demonstrate the effect of external stimuli on defect-induced magnetization and the impact of strain and electrical gating on the defect-induced magnetization. Finally, Sec. IV explores the theoretical aspect of understanding how defects influence magnetism in oxide materials. The review is ended with a summary and outlook on material design and experimental and theoretical techniques.

II. DEFECT-INDUCED MAGNETISM

A. Crystal defect- and dopant-induced magnetism

Introducing defects and dopants into oxides can alter their magnetic properties in various ways. There are three types of defects in a crystal: point defects, line defects, and plane defects. Point defects include vacancies (missing atoms), anti-site disorder (where atoms are swapped in the lattice), and two kinds of impurities: interstitial (atoms positioned in the spaces between the regular lattice points) and substitutional (foreign atoms replacing host atoms in the lattice). These impurities are often introduced through doping. Doping, the process of adding impurities to a material, is a key method for manipulating the magnetic characteristics of oxides. We can categorize the dopants into two groups: those that are naturally magnetic (like iron, nickel, and cobalt) and those that are not (such as hydrogen, helium, and lithium). These categories lead to two doping strategies. The first involves incorporating magnetic elements into the oxide, potentially forming magnetic order (like ferromagnetism or antiferromagnetism) when these elements are present in sufficient quantities. The second strategy uses non-magnetic dopants to modify the inherent magnetic properties of the oxide material itself. Line and planar defects in crystals refer to one-dimensional imperfections, such as dislocations, and two-dimensional (2D) imperfections, such as grain boundaries and hetero-interfaces. Such structural defects can break the local symmetry, alter the electronic structure, or effectively trap charges as they enable more energetically favorable to accommodate charged defects, clusters, or dopant ions.[16–18] This can lead to the occurrence of emergent ferromagnetic phenomena, including localized magnetic moments,[19–22] long-range magnetic ordering,[23] and anisotropic magnetic ordering,[24] observed at or near these structural defects in oxide materials that are typically non-magnetic in their defect-free states. In the following subsections (Secs. II A 1–III A 4), we will discuss separately how different types of defects induce and tune the magnetism of various oxide systems.

1. Point defects

The properties of functional metal oxide nanostructures can be highly susceptible to the presence of V_O defects. The defect concentration in these systems plays an important role in tuning ferromagnetism, and therefore, investigations on the magnetic and structural properties of some types of transition metal-doped semiconductors were carried out. $SrTiO_3$ (STO) is a key prototypical member of the perovskite oxide family, which is susceptible to the effect of V_O.[8,25–27] STO is a transparent insulator with an indirect bandgap of 3.2 eV at room temperature (RT),[8,25,26] where the 2p oxygen (O) valence band is separated from the 3d titanium (Ti) t_{2g} conduction band. In its tetragonal structure, bulk STO exhibits properties of incipient ferroelectrics or quantum paraelectrics at low temperature (<50 K).[8,26,28] These properties are particularly interesting due to the high dielectric constant, low dielectric loss, and susceptibility to tuning by applied electric fields and temperature changes.[8,25,26,28,29] In STO, V_O donates electrons to the crystal and are thus believed to be responsible for the magnetism of the system. While interstitial oxygen and defects related to cation-oxygen anion pairs lead to magnetism, these defects have higher formation energies.[30] They can be introduced by heating the crystals in a vacuum,[31–34] which creates a neutral defect accompanied by two electrons. Different arrangements of oxygen vacancies, each carrying distinct charges, frequently create localized states. These states possess unpaired spins within the energy gap of the material.[34,35] These localized states, arising from oxygen vacancies, can present themselves in two forms at the bottom of the conduction band: they can either be unpolarized, meaning the spins of the electrons are randomly oriented, or spin-polarized, where the electrons have aligned spins. Typically, these electrons form small and large polarons,[34,36] impacting the material's magnetic and electronic properties.

Recent progress in thin film technologies has enabled precise manipulation of the atomic composition in oxide thin films. This property is achieved by carefully controlling the growth parameters during the film's development. Such precision allows for the emergence of unique and interesting physical properties in these materials, including significantly enhanced ionic and electronic conductivity,[37] high-temperature ferroelectrics,[37,38] and room-temperature magnetism.[34,39–43] For example, the presence of charged atomic point defects (e.g., vacancies and/or interstitials) in oxide thin films can trigger significant atomic/electronic rearrangement of systems that contain d- and/or f-orbital cations.[37,39,41] This results in the generation of unexpected RT ferromagnetism (FM), often referred to as $d0$ ferromagnetism, observed in non-magnetic oxides, e.g., TiO_2, SnO_2, ZnO, HfO_2, and $SrTiO_3$.[6,12,37,39–41,44] This type of magnetism is characterized by non-trivial FM moments, limited defect threshold concentration within host oxide lattices, high Curie temperatures (T_C) well above RT, and often exhibits magnetic anisotropy.[6,12,37,39–41,44] It was suggested that the behavior of these materials is due to (i) the formation of defect-associated impurity bands that become spin-polarized and/or (ii) FM interactions between the impurity band and the surrounding d/f states of host cations and/or (iii) contribution of collective orbital moments.[6,37,45] Currently, a significant amount of research focuses on understanding the microscopic causes of magnetic interactions and patterns.[6,46] This research involves precisely managing the distribution and concentration of point defects within various crystalline oxide structures.

Additionally, there is an increasing effort to control the growth of oxide films carefully and thereby their properties.[6,12,37,41,47] For example, in a non-magnetic stoichiometric TiO_2 film where titanium exists in its Ti^{4+} state, introducing V_O can lead to Ti^{3+} or even Ti^{2+} states.[45,48] Both states possess unpaired 3d electrons, giving rise to a magnetic moment. Yttrium manganese oxide ($YMnO_3$ or YMO), a hexagonal multiferroic oxide, is another example that shows emerging ferromagnetism with the introduction of V_O.[49] This effect can result in a non-zero magnetization along its c-axis. YMO's response to V_O underscores the diverse impacts that defects and doping can have on the magnetic properties of oxides.

Among the various film growth methods, pulsed laser deposition (PLD) has been widely used for growing thin oxide films over the past two decades.[8,37,50,51] PLD allows the growth of diverse oxide thin films with a control at the level of single atomic layers, offering high flexibility in the choice of materials and parameter tunability. In the PLD system, two factors play crucial roles in depositing materials onto substrates: the intensity of the laser (laser fluency) and the interaction between the vaporized materials species (plume) and the surrounding gas. These factors significantly influence how the ablated (vaporized) species are transferred onto the substrates, particularly at the right temperature.[8,37] Thus, inappropriate or non-optimized PLD parameters can result in non-uniform vaporization (noncongruent ablation) and variations in the paths (trajectories) of atoms and ions based on their mass as they move through the laser-generated vapor cloud (laser plume).[8,37] Thus, the key to producing non-stoichiometric films with controlled atomic defects lies in these parameters' simultaneous and precise control, see Fig. 2. This control is essential for transferring material from the ablated targets to the films and studying the effects of atomic defects in the grown films.[8,37] The oxygen pressure level is a critical parameter in the PLD growth chamber. It significantly influences the behavior of vaporized materials, known as ablated species. This directly affects various aspects of the film's growth dynamics: oxygen stoichiometry, and the interactions, collisions or desorption among different components in the growth process. All of these factors affect the film growth.

(1) In a vacuum-like environment, where interactions with background gas are minimal or absent, very high-energy particles (over 1000 eV) move toward the substrate—this "*ballistic mode*" results in different arrival times for the species due to their varying energies.
(2) In a "*transition-like*" regime, which occurs at certain pressure ranges (5×10^{-3} mbar to 5×10^{-2} mbar), the mean free path of the species is smaller than one-tenth of the distance from the target to the substrate. Here, chemical reactions between the background gas and the plasma plume are possible. The arriving species maintain relatively high kinetic energies at the substrate in this setting.
(3) Lastly, at high oxygen pressures (e.g., 1×10^{-1} mbar), the expansion of the plume is significantly slowed down. The background gas confines the plume interacting ablated species, leading to a collective movement.

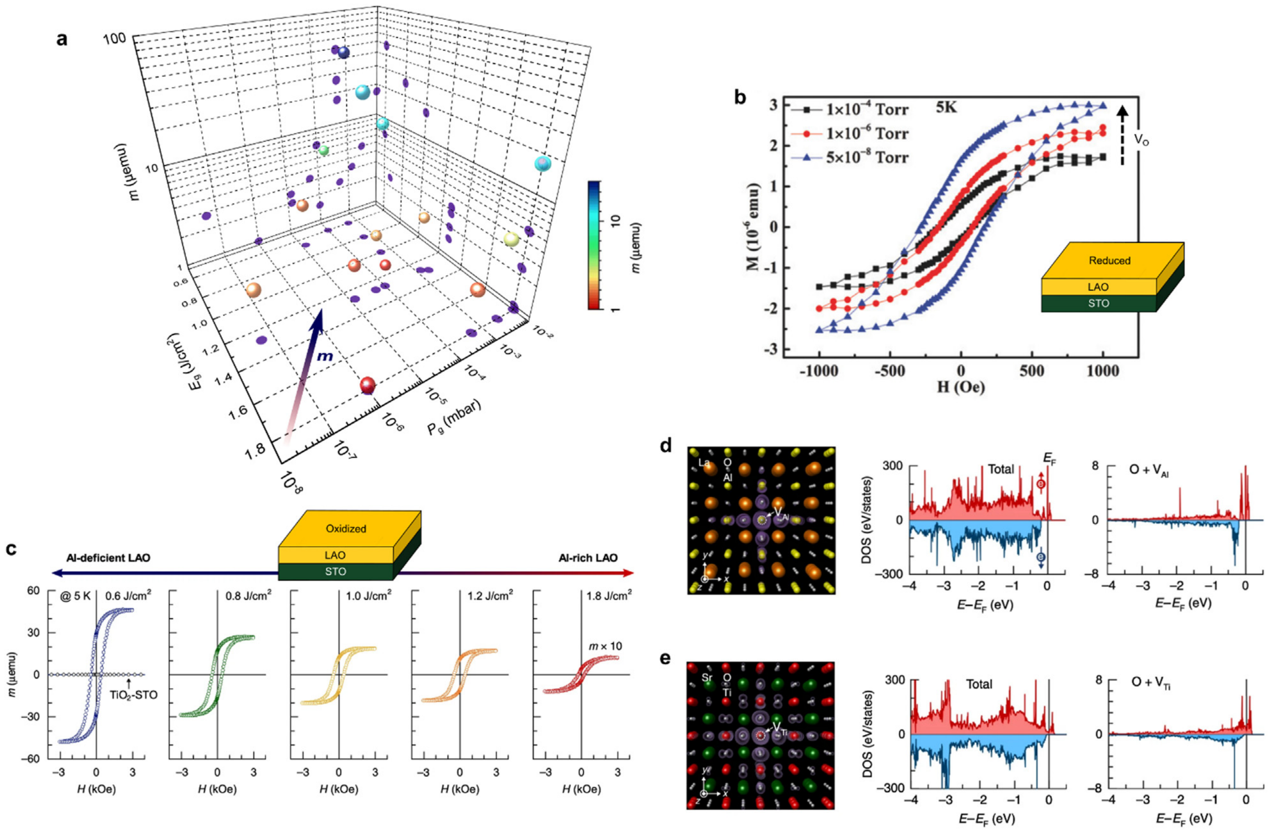

FIG. 2. (a) A comparison of the saturation magnetic moment (m) of LAO/STO samples grown by various PLD growth parameters: laser fluence (E_g), oxygen partial pressure (P_g).[12] (b) Magnetic hysteresis loops of 24 UC-LAO/STO samples grown at different P_g to examine the effect of V_O. The films were grown by a constant E_g (=1.275 J/cm^2.[62] (c) 5 K magnetic hysteresis loops of the oxidized 9-u.c. LAO/STO samples as a function of E_g. After film growth, all the grown samples were cooled down to RT in O_2 (200 mbar). (d) and (e) B-site cation vacancy induced magnetization (left) and the total spin-polarized density of states (right) near the valence band states for LAO with V_{Al} (d) and STO with V_{Ti} (e), calculated by first-principles DFT.[12]

Hence, the background oxygen pressure is a vital growth parameter that determines the growth dynamics and chemical plasma composition of oxide films, especially in the case of complex oxide film growth.[8,27,52] In addition, for the PLD growth of complex compound oxides, a dissimilar ablation with an inadequate fluence that can preferentially ablate particular elements causes the formation of cation non-stoichiometric oxide films. Thus, a delicate tuning of laser fluence under appropriate oxygen partial pressure effectively induces and controls desired cation and/or oxygen defects in PLD films to create defect-mediated physical and chemical properties [Figs. 2(b) and 2(c)].[8,12,34,48,53–62] This effect is due to a preferential ablation of relatively lighter cations that can be induced by increasing laser fluence during PLD film growth, leading to a cation non-stoichiometric film.

The following discussion will compare various point defects and their related magnetic properties. This comparison will be made with the growth characteristics of complex oxide heterostructures. These heterostructures are created by precisely controlling the parameters in the PLD process.

(i) *The effect of V_O in oxide films*: it is widely believed that V_O is the electron source to induce the RT magnetism in various oxide film materials/heterostructures such as STO,[8] TiO_2,[58] and $LaAlO_3$(LAO)/STO interface.[54,55] The V_O content in the oxide films is controlled by lowering the oxygen environment during film growth or by changing the temperature of the grown films (e.g., ex situ annealing in a vacuum). For example, V_O in STO can partially reduce Ti^{4+} into magnetically active Ti^{3+}.[34,56,57] *Coey* et al.[34] suggested that the origin of ferromagnetism in reduced STO is either due to direct exchange interactions between V_O and the molecular orbitals of valence electrons of surrounding Ti ions or due to a Stoner-type spin-splitting of the Ti 3*d* band for ferromagnetically coupled electrons. However, Brovko and Tosatti reported theoretical results suggesting that an isolated V_O defect in STO only stabilizes states with low or zero total magnetization since the two Ti spins facing each other across the V_O are antiferromagnetically coupled via strong direct exchange interaction.[56] Doennig and Pentcheva theoretically demonstrated that in LAO/STO heterostructures, Ti d_{xy} bands could be dominantly magnetized via magnetic double-exchange interactions between Ti^{3+} and Ti^{4+} when a tensile in-plane strain is induced in TiO_6 octahedra and the electron doping level is below $7 \times 10^{14}\ cm^{-2}$.[57] However, this electron doping level (0.5e per Ti) per STO monolayer is hard to achieve practically when considering that Ti d_{xy} orbital polarization in a c-axis compressed STO is purely induced by a high V_O concentration of about $\sim$25 at. % as a V_O sublattice. Note that it was found that the perovskite lattice of $SrTiO_{3-x}$ retains its structure even at a V_O concentration of $\leq$5.6 at. %. Similar V_O-mediated Ti magnetization levels have been observed experimentally in reduced STO thin films,[8] STO-based heterostructures (e.g., LAO/STO interfaces),[59] and reduced TiO_{2-x}.[50] However, these examples usually show weak magnetic responses, which do not appear robust enough to be employed practically.

(ii) *The effect of V_C in oxide films*: For the last decades, the effect of V_C on the generation of magnetism has been consistently observed in various binary, ternary, and complex oxide systems with noticeable magnetic moments ($m > 1 \times 10^{-5}$ emu) and high T_C (e.g., $\gg$300 K).[6,12,45,58] Such cation vacancy-induced magnetism was manifested when the associated magnetism was found in both *n*- and *p*-type films/heterostructures without V_O.[12,63] Theoretical and experimental studies demonstrated that both the Ti and O vacancies could contribute to the magnetism of the STO system.[8,53] However, it was shown that the Sr vacancy cannot induce noticeable magnetism in STO.[53,60] Recently, Park *et al.*[37] reported tunable magnetism in non-magnetic ABO_3-perovskite $LaAlO_3$, $SrTiO_3$ films, and their heterostructures via creating and controlling B-site cation vacancies (V_{Al} and V_{Ti}) [Figs. 2(d) and 2(e)].[8,37] The formation of V_{Al} and V_{Ti} happened in the LAO and STO layers by employing low laser fluence during film growth, resulting in preferential scattering of the light plume species. This effect results in Al-deficient LAO (Ti-deficient STO) films under relatively low laser fluencies (e.g., 0.6 J/cm^2). Their theoretical calculations clarify that the V_{Al} and V_{Ti} act as *p*-type defects and, thus, create acceptor-like states near the valence band of LAO and STO. The cation vacancy defects are not spin-polarized, but they induce spin polarization of the neighboring host ions, especially for the six nearest oxygen ions. This effect was experimentally probed by observing a reversible polarization of O states at O *K*-edge X-ray magnetic circular dichroism, measured by swapping the applied fields, $B = +6$ and -6 T. Similar defect band formation and oxygen spin polarization were found in ZnO, MgO, and TiO_2 with cation vacancies, supported by theoretical studies.[12,45,48]

2. *Topotactic phase transitions: V_O-induced magnetism*

Next, we will focus on the effect of ordered atomic vacancies/inclusions and rearrangement in a crystal lattice, which lead to a long-range ordered structural phase change, known as a topotactic phase transition. Such transitions have the potential to give rise to new phases in oxides with rare valent states of the constituent metal ions. For instance, the ABO_3 perovskite (PV) structure can be transformed to a brownmillerite (BM) one, mediated by a long-range ordering of oxygen vacancies, as schematically shown in Fig. 3(a).[31] This transition occurs by removing 1/6 of the oxygen atoms from the perovskite lattice. The BM structure has alternating layers: one has BO_6 octahedra and the next has oxygen-deficient BO_4 tetrahedra. This type of transition provides a controllable manner of exploring V_O-controlled functionalities.[31] This is in contrast to the dilute V_O discussed in the previous section (Sec. II A I).

Topotactic reduction reactions of various epitaxial oxide films (e.g., growing the lowest oxidation state of EuO from the higher oxidation states such as Eu_3O_4 or Eu_2O_3) have been extensively demonstrated by carefully controlling the oxygen stoichiometry during film growth.[64,65] Among all film growth parameters, critical growth parameters are the careful use of both sufficient growth temperature (depending on materials) and appropriately low P_O conditions in ultrahigh or high vacuum deposition equipment such as molecular beam epitaxy (MBE),[64] magnetron sputtering, and PLD.[65,66] These conditions are essential for achieving phase-pure growth and effective oxygen reduction. However, structural conversions to polymorphic phases (with the occurrence of impurity phases) can thermodynamically occur

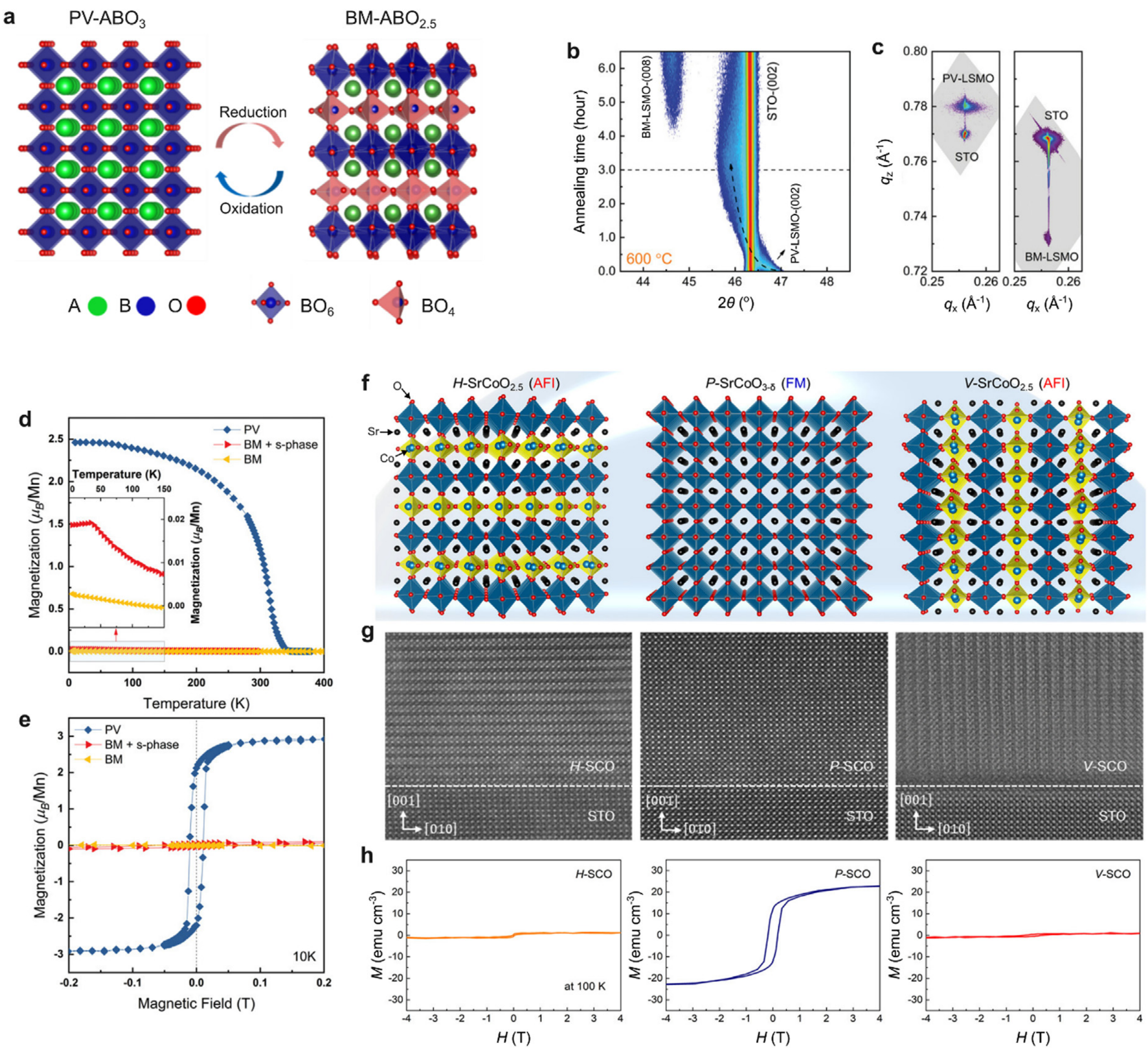

FIG. 3. (a) Schematic diagram of topotactic phase transition from perovskite (PV)-ABO_3 to brownmillerite (BM)-ABO2.5 structure, and vice versa.[31] (b) *In situ* XRD of epitaxial PV-LSMO thin film on a STO substrate, measured during vacuum annealing at 600 °C. (c) Reciprocal space maps of the pristine PV-LSMO (left) and transformed BM-LSMO (right), measured around the STO(103) reflection. (d) Temperature-dependent magnetization of the PV-LSMO phase, BM phase with a surface (S) phase, and pure BM phase, measured by applying an in-plane magnetic field of 10 mT.[73] (e) In-plane magnetic hysteresis loops for the various LSMO phases, measured at 10 K. (f) Crystal structure of BM-$SrCoO_{2.5}$ having a horizontal oxygen vacancy ordering (H-$SrCoO_{2.5}$) (left), PV-$SrCoO_3$ (middle), and BM-$SrCoO_{2.5}$ having a vertical oxygen vacancy ordering (V-$SrCoO_{2.5}$) (right). These phases have been transformed by ionic liquid gating. (g) The corresponding high-angle annular dark field scanning transmission electron microscopy images of H-$SrCoO_{2.5}$ (left), PV-$SrCoO_3$ (middle), and V-$SrCoO_{2.5}$ (right). (h) The corresponding in-plane magnetic hysteresis loops of the antiferromagnetic H-$SrCoO_{2.5}$, ferromagnetic PV-$SrCoO_3$, and antiferromagnetic V-$SrCoO_{2.5}$, measured at 100 K.[226]

when lower growth temperatures or inappropriate P_O conditions are employed.

For the film growth of brownmillerite $SrCoO_{2.5}$ (BM-SCO)[66] and $SrFeO_{2.5}$ (BM-SFO),[67] Jeen *et al.*[66] reported optimal growth conditions for phase-pure BM-SCO with a narrow growth window of P_O $\sim 1 \times 10^{-2}$ to $\sim 3 \times 10^{-1}$ mbar at a temperature of 750 °C. Outside this growth window, lower growth temperature (<750 °C) and depositions at $P_O < \sim 1 \times 10^{-5}$ mbar resulted in the formation of rhombohedral $Sr_6Co_5O_{15-\delta}$ and additional CoO_x impurity phases. In addition, *Jeen* et al.[66] performed *in situ* post-annealing with high P_O ($\sim 100 < P_O \leq \sim 300$ mbar) after the BM-SCO film growth, inducing a topotactic oxidation to form the PV-SCO phases. *Khare* et al.[67] reported the growth of BM-SFO films at a P_O of 1.3×10^{-2} mbar and at a growth temperature of 700 °C, followed by post-annealing with various P_O (1.3×10^{-2}–6×10^{2} mbar) mbar for 10 min. Their results showed that the BM-phase SFO remains stable till $P_O \leq \sim 1 \times 10^{-1}$ mbar. Similarly, epitaxial BM-$LaCoO_{2.5}$ films were successfully grown in PLD at 665 °C–700 °C under P_O of $\sim 1 \times 10^{-1}$ mbar as reported by Li *et al.*[68] and Choi *et al.*[69]

An alternative approach to inducing the BM phase involved using oxygen-getter layers during film growth. Ferguson *et al.*[70] demonstrated topotactic oxygen reductions in various manganite-based heterostructures by employing oxygen-getter layers. In their study, manganite films—including PV-LSMO (grown at 615 °C in $P_O = 1.3 \times 10^{-1}$ mbar), $La_{0.7}Ca_{0.3}MnO_3$ (615 °C, $P_O = 1.3 \times 10^{-1}$ mbar), $Pr_{0.7}Ca_{0.3}MnO_3$ (850 °C, $P_O = 1.3 \times 10^{-1}$ mbar), and $LaMnO_3$ (830 °C, $P_O = 4 \times 10^{-1}$ mbar)—were initially grown under oxygen-rich conditions. Subsequently, a 6-unit cell (uc) of oxygen deficient $SrTiO_{3\text{-}\delta}$ in 1.3×10^{-4} mbar was grown on the top of the oxygenated 21.2 uc-LMSO film, and the films were then capped by the variable thickness of $LaAlO_{3\text{-}\delta}$ (LAO) (620 °C, 1.3×10^{-4} mbar). The results show an increase in the structural transition from the PV-LSMO phase to BM one, pronounced after the growth of ∼6 UCs of LAO capping layer. It was also found that the "oxygen getter layer"—grown at temperatures as low as 415 °C under 1.3×10^{-5} mbar and as high as 615 °C in 1.3×10^{-1} mbar for the case of STO—facilitates the formation of the BM LSMO.

An important mark is that the V_o ordering in the BM phase lattices is highly sensitive to the epitaxial strain, induced by the underlying layers/substrates during film growth. Various studies have been explored the direct growth of BM phases on different lattice-mismatched substrates. Choi *et al.*[69] reported a clear observation on the epitaxial strain-dependent V_O ordering for 30 nm-thick $LaCoO_{3-\delta}$ films, grown under strains of −0.3% ($LaAlO_3$), +1.7% (LSAT) and +2.6% ($SrTiO_3$). Compressive strain leads to V_O ordering parallel to the substrate, while tensile strain leads to V_O ordering perpendicular to the substrate. Similarly, Hu *et al.*[71] demonstrated that the substrate-induced strain determines the V_O ordering in LSMO. Under compressive strains of −2.27% (LAO) and −0.2% (LSAT), V_O ordering aligns parallel to the substrate surface. In contrast, an initial V_O ordering perpendicular to the substrate surface was observed under a tensile strain of +1.8% ($DyScO_3$).

The topotactic transformation from the ABO_3-PV oxides to the BM phase is carried out by external treatments, e.g., vacuum annealing and ion beam irradiation.[72] In the case of manganites (e.g., $La_{0.7}Sr_{0.3}MnO_3$), a sufficient high P_O ($\sim 1 \times 10^{-1}$ mbar) is typically required to preserve the oxygen stoichiometry during film growth, stabilizing an initial PV phase.[70] To realize the topotactic reductions to the BM phase, various post-annealing processes have been explored to identify the optimal conditions.[71,73,74] A study by *Cao* et al.[73] utilized high oxygen pressure sputter deposition (HOPSD) to grow PV-LSMO at 500 °C and subsequently post-annealed the grown samples from 200 to 600 °C under 10^{-6} mbar. Their *in situ* XRD results directly show the topotactic transition from the PV to the BM one over a period of 63h. Hu *et al.*[71] also investigated the PV-to-BM phase transition by growing PV-LSMO and performing post-annealing LSMO-lamella during *in situ* STEM measurements. The PV-LSMO was grown at 625 °C in 1.3×10^{-1} mbar and subsequently *in situ* annealed at 500 °C in 1 atm for 15 min. It was shown that the PV to BM phase transition occurs at 500 °C under a vacuum of 1.3×10^{-9} mbar. Additional details can be found in a study by Nukala *et al.*,[74] where PV-LSMO capped with $Hf_{0.5}Zr_{0.5}O_2$ was grown at 775 °C in 1.3×10^{-1} mbar.[75] Their *in situ* TEM annealing experiments reveal deoxygenation of MnO_6 to MnO_5 at temperatures as low as 150 °C. At 300 °C, the formation of the BM phase was clearly observed. However, when the annealing temperature was increased above 400 °C, Ruddlesden-Popper phases were formed due to the loss of Mn cations.

Ion beam radiation has proven to be an effective method for inducing preferential oxygen sputtering in PV oxides, facilitating topotactic phase transformations. Ferreiro-Vila *et al.*[72] presented a topotactic transformation from originally PV $SrFeO_{3\text{-}\delta}$ films (semiconducting) to the BM $SrFeO_{2.5}$ phase (relatively insulating) using Ga^+-focused ion beam (FIB) irradiation. By selectively removing oxygen atoms from PV $SrFeO_{3\text{-}\delta}$ films through FIB irradiation, the irradiated areas were transformed into the BM phase. Various irradiation parameters were investigated, including ion doses of 3×10^{13} and 3×10^{16} ions/cm^2 at 5 kV ion acceleration energy, and 7.2×10^{13} and 3.6×10^{16} ions/cm^2 at 30 kV. The results indicated that low-dose Ga^+ irradiation ($\sim 10^{14}$ ions/cm^2) combined with high ion energy (30 kV) effectively induced the topotactic phase transition within shorter irradiation times of 1–10 s. Conversely, high-dose Ga^+ irradiation led to amorphization of the crystal structure. Furthermore, the irradiation-induced phase transition from BM to PV was reversible upon annealing at 300 °C in P_O 0.4 mbar. This method offers technical advantages such as rapid processing and high-resolution patterning for creating topotactic phase areas, potentially applicable to other oxide materials.

The phase transition from the PV phase to the BM phase results in significant changes in physical properties [Figs. 3(b) and 3(c)]. For example, the PV-$La_{0.7}Sr_{0.3}MnO_3$ (PV-LSMO) changes from ferromagnetic semimetal to an antiferromagnetic insulator in its BM form, BM-$La_{0.7}Sr_{0.3}MnO_{3\text{-}x}$ (BM-LSMO) [Figs. 3(d) and 3(e)].[73] Topotactic phase transitions are predominantly observed in transition metal oxides such as those containing vanadium (V), manganese (Mn), iron (Fe), cobalt (Co), and nickel (Ni).[31,76] This prevalence is attributed to the variable valence states readily accessible in these elements. Notably, the topotactic transformations exhibit strongly tunable magnetic properties.[76,77] Examples will be discussed for the cases of spin state change, magnetic ordering, magnetic anisotropy and magnetic phase transition:

(i) **Spin State Changes:** A notable example illustrating the impact of topotactic phase transitions on the spin state and magnetic properties of transition metal oxides is observed in the perovskite $La_{0.5}Sr_{0.5}CoO_3$.[78] Analysis of soft X-ray absorption spectroscopy (XAS) spectra on these materials reveals a distinct shoulder at around 780.5 eV in the PV phase, indicative of coexistence of high-spin/low-spin (HS/LS) states in Co^{3+} configuration $t^6_{2g}e^0_g/t^4_{2g}e^2_g$) and a high-spin state in Co^{4+} ions (configuration $t^3_{2g}e^2_g$).[77,79] Following a topotactic phase transition to the BM phase in $La_{0.5}Sr_{0.5}CoO_{2.5}$, notable changes are observed in the XAS spectra. Specifically, the main peak of the Co $L_{2,3}$ edges shifts to lower energy by over 0.7 eV, indicating the transition of Co to a lower oxidation state. Coupled with the O *K*-edge spectra analysis, the authors of this manuscript deduced that the Co ions in the tetrahedral layers of BM-$LaSrCoO_{2.5}$ undergo a spin state transition from high spin state to a low spin/intermediate spin state concurrent with the topotactic phase transition. This effect is evidenced by the diminishing O *K*-edge pre-peak in the BM phase, which is utilized to probe the unoccupied O 2*p* density of states hybridized with Co t_{2g} orbitals.[77,79] The transition influences the magnetic behavior of the material, resulting in the FM-AFM phase transition. Moreover, first-principles calculations on $SrCoO_3$

(SCO) films demonstrate a similar phenomenon,[31] where the spin state of Co ions transitions from a Co^{4+} intermediate state to a Co^{3+} high spin state. In both cases, these transformations profoundly affect the macroscopic magnetic properties of the materials during the topotactic phase transition.

(ii) **Magnetic Ordering:** In transition metal oxides experiencing topotactic phase transitions, the magnetism is influenced by the interactions between magnetic ions, which are mediated by oxygen ions situated between them.[80] The presence of V_O disrupts these interactions altering the material's magnetic ordering. Li *et al.*[31] show profound changes in magnetic ordering when a FM, metallic $La_{0.7}Sr_{0.3}CoO_3$ is reduced to AFM, long range ordered BM $La_{0.7}Sr_{0.3}CoO_{2.5}$. The magnetic ordering is further rearranged when the Co sites are reduced, forming a ferromagnetic insulator (FMI) phase in $La_{1.4}Sr_{0.6}CoO_4$, a single-layered perovskite. Additionally, the transition between the perovskite and BM phases is accompanied by a gradual lattice expansion due to the introduction of oxygen vacancies (V_O). Huang *et al.*[81] systematically examine the correlation between magnetic ordering and lattice parameters for the reduction of $LaCoO_3$. They show that the magnetization is intricately linked to the out-plane lattice constant. This observation aligns well with the theoretical model, which suggests that an increased Co–Co distance leads to diminished *d-p* hybridization between *d* orbital in transition metal ions and *p* orbital in oxygen ions. This altered the magnetic ordering from a ferromagnetic state to an anti-ferromagnetic state.[31] This phenomenon is commonly observed in many other topotactic transition oxides, as evidenced in compounds such as $SrMnO_3$[82] and $Nd_{0.5}Sr_{0.5}MnO_3$.[83]

(iii) **Magnetic Anisotropy:** The crystal structure of oxide materials often determines the magnetic anisotropy, which describes the orientation-dependent magnetic behavior.[84] Topotactic transformations that maintain ordered crystal planes can preserve or alter the magnetic anisotropy of the material. This effect, in turn, affects how the material responds to external magnetic fields. For instance, Walter *et al.*[85] fabricated $La_{1-x}Sr_xCoO_{3-\delta}$ thin films on various substrates for tensile and compressive strain in the range of +1.8% to −2.1%. These strains lead to the ordering of V_O rich planes parallel to the substrate for compressive strains and perpendicular for tensile strains. The magnetic anisotropy in the BM phase is perpendicular to the perovskite planes, leading to an out-plane magnetic anisotropy under compressive strain and in-plane magnetic anisotropy under tensile strain. The in-plane V_O ordering makes the thin film exhibit a pronounced perpendicular magnetic anisotropy, which is rarely reported in many perovskites.[85] The mechanism for perpendicular anisotropy in perovskite with ordered V_O remains controversial. Still, it was suggested that the interfaces between CoO_4 tetrahedra and CoO_6 octahedra play a key role in tunable magnetic anisotropy. These interfacial interactions imply that V_O in one of the layers can influence the magnetic anisotropy in an adjacent layer. This effect is exemplified in the LSMO/$SrCoO_{3-\delta}$ heterostructure, where LSMO layer shifts from in-plane magnetic anisotropy to perpendicular magnetic anisotropy when the $SrCoO_{3-\delta}$ layer is transformed from the PV-$SrCoO_3$ phase into the BM-$SrCoO_{2.5}$ phase.[31]

(iv) The tunable perpendicular magnetic anisotropy observed in perovskite/brownmillerite ($A'B'O_3/A''B''O_{2.5}$) heterostructures is attributed to interfacial atomic misalignment.[86] In such structures, the $B'O_6$ octahedra in the perovskite layer tend to share apical oxygen atoms with BO4 tetrahedra in the brownmillerite layer, minimizing the system's total energy. This behavior, confirmed experimentally and theoretically,[87,88] leads to the elongation of the octahedra along the *z*-axis, facilitating orbital reconstruction and enhancing the out-of-plane magnetic anisotropy in the perovskite layer. Similar modulation of magnetic anisotropy via atomic reconfiguration at interfaces has been reported in various other perovskite/brownmillerite systems, such as $LaBaMnO_3/SrFeO_{2.5}$ and $LaSrCoO_3/LaSrMnO_{2.5}$.[89] Leveraging this strategy, researchers have demonstrated reversible control of magnetic anisotropy using topotactic phase transitions. For example, in $LaSrMnO_3/SrCoO_{2.5}$ heterostructures, ionic gating is employed to insert or extract oxygen ions in the $SrCoO_{2.5}$ layer to induce topotactic phase transitions.[31] Accompanying these transitions, the magnetic anisotropy in the underlying LSMO layer shifts between in-plane and out-of-plane orientations, consistent with the lattice structure changes in the SCO layer.

Magnetic Phase Transitions: Some topotactic transformations can induce magnetic phase transitions in oxide materials. During topotactic phase transitions in transition metal oxides, magnetism is predominantly governed by double exchange and superexchange interactions, where magnetic ions interact through oxygen ions in the form of M-O-M (M represents metal ions).[90] The induction of oxygen vacancies facilitates unique magnetic phase transitions in these materials. For example, in $LaMnO_3$, the Mn ions are typically in the Mn^{3+} state, engaging in antiferromagnetic ordering via superexchange interactions, i.e., Mn^{3+}-O-Mn^{3+}.[91] However, during the formation of the BM phase, the introduction of oxygen vacancies leads to converting some Mn^{3+} ions into Mn^{2+}, a process necessary to maintain charge neutrality.[91] The interactions between Mn ions are thus predominantly governed by the double exchange mechanism between Mn^{3+} and Mn^{2+}.[92,93] As a result, the AFM ordering transitions to an FM phase during the topotactic phase transition.

Furthermore, interest in the functionalization of the topotactic phases has led to the demand for controlling the transition at room temperature under (near) ambient conditions. Leveraging the substantial electric double layer at the electrolyte/oxide interface, studies have shown that electrolyte gating—comprising an ionic conductor electrolyte and correlated oxides with a tunable phase structure—can effectively induce topotactic phase transitions at around RT.[94,95] Han *et al.*[226] reported a topotactic phase transition starting from epitaxial BM-SCO films with horizontal V_O ordering, into vertical V_O ordering by implementing ionic liquid gating [Figs. 3(f)–3(h)]. A phase change of the AFM insulating BM-SCO films to the FM conductive P-SCO was observed when negative gating voltages were applied to the thin film. Conversely, using positive gating voltages, the P-SCO films transform into AFM-insulating BM-SCO films, but with vertical V_O orderings. The vertical alignment of V_O orderings in the BM-SCO films results from a vertical pathway of O under electric fields. The above discoveries highlight the potential of manipulating topotactic phase transitions and V_O arrangements to alter the magnetic properties of transition metal oxides. However, ionic liquid-based electrolytes are limited by their mechanical strength and fluidity.[96] Replacing these with solid-based electrolytes that offer comparable ionic conductivity could overcome these limitation.[97] Other alternative approaches involves the surface decoration of perovskite oxides with noble metals.[98] These metals can effectively weaken the metal-oxygen chemical bonds, even at room temperature, offering a viable method for controlling the phase structure of oxides. Other lesser-explored methodologies include exploiting the oxygen diode phenomenon in heterostructures,[99] where differing oxygen affinities between two oxides allow for the unidirectional flow of oxygen ions.

The topotactic phase transition in oxides has been well studied for oxides and keeps showing a rich host of magnetic properties. The topotactic phase transitions can be readily controlled during growth and post-growth. Utilizing the topotactic phase transition for practical applications requires the functionalization of this phase transition itself under ambient, room temperature conditions. This functionalization is an area of ongoing fascinating and creative research.

3. Dopants: Interstitial and substitutional

Interstitial light elements such as B_i, C_i, and N_i (where the subscripted "*i*" denotes interstitial) can generate non-trivial magnetic properties in materials with unique lattice, charge, and spin arrangements. These elements serve dual purpose: they affect the crystal structure's stability and adjust the intrinsic magnetic properties. When present in small quantities, these interstitial light elements can stabilize otherwise thermodynamically unstable crystal structures and lead to an expansion of the unit cell volume. They impact the interatomic distances between host ions and influence the orbital hybridization between the host ions and interstitials. This interaction facilitates the fine-tuning of intrinsic magnetic properties. Altering the structure through interstitial doping is closely connected to the resultant magnetic ordering.

The effect of interstitials has been widely found in magnetic metal alloys. For instance, in rare-earth Fe-based magnets, a longer Fe–Fe distance induced by including B_i, C_i, and N_i favors the FM states from initial antiferromagnetic states.[100,101] This results from smaller overlapping of 3*d* wave functions and the subsequent reduction in the exchange interaction. Additional insights on interstitial atoms in magnetic metal alloys can be found in a previous review article by Kitagawa *et al.*[100] Alteration of the magnetic properties by interstitial atoms is not limited to metal alloys and was reported in oxide materials. An example is the RT-FM response in C-doped ZnO films[102] and nanowires.[47] Wang *et al.*[47] suggested that the enhancement in the FM moment of the system is associated with the stabilization of C_i atoms, together with V_{Zn} defects, created by ion implantation [Figs. 4(a)–4(d)]. Furthermore, they found that additional moments arise from individual atoms bonded with the neighboring O atom. In addition, Park *et al.*[37] found that interstitial B_i atoms induce an RT-FM in non-magnetic insulating LAO, as confirmed experimentally and theoretically, see Figs. 4(e)–4(i). The B_i atoms create new *s*- and *p*-states near the Fermi level of LAO. Of particular interest is the fact that the delocalized spin-polarized electron provided by the *p*-state of the B_i is partially transferred to the neighboring host atoms. This situation is primarily driven by the alignment of the spin-polarized electrons between the B_i and La atoms through *p*-*d* band hybridization, resulting in a non-zero magnetization of the system. A limited B_i concentration of 3.2 at. % induces RT-FM in the LAO system. In a subsequent study, the effect of B_i was also found in $LaAlO_3$:$LaBO_3$ (LABO) nanocomposite films grown STO(001) single crystals.[42] The transient formation of the 2D-to-3D vertically aligned LABO/STO(001) heterostructure is driven by the misfit strain-mediated phase separation of miscible LAO and LBO oxide phases through strain relaxation processes. The effective magnetic ordering of La-B_i-La was induced along the out-of-plane direction, as hinted, on the one hand, by the measurement of a magnetic anisotropy, which is not observed in undoped LAO and LBO, and on the other hand, by the establishment of an LAO:LBO vertically aligned nanopillar structure. The effect of interstitial light elements on the magnetism of oxide materials, either in bulk or film form, is relatively new and not well established, and it provides a promising avenue for engineering highly functional magnetic materials via elemental technology. Incorporating interstitial light elements during oxide film growth typically requires specific growth conditions due to their volatile and diffusive nature and tendency to undergo oxidation and clustering. For instance, when using PLD, it could be required to employ relatively low temperature, high laser fluence, and low P_O to prevent detrimental effects associated with oxidation and clustering during the film growth process.[34]

Concerning substitutional dopants, fascinating magnetic symmetry breaking can be evidenced in oxides, such as $SrVO_3$ (SVO) and $EuTiO_3$ (ETO). Specifically, ETO displays paramagnetic phases due to two key factors: the breaking of positional symmetry caused by octahedral rotations, and the breaking of magnetic symmetry resulting from spin disorder.[103] ETO is a *G*-type antiferromagnet in its bulk form, with each Eu site having a spin moment of $J = S = 7/2$.[104] This antiferromagnetic order can transition to a ferromagnetic order through, among other things, epitaxial strain,[105,106] chemical doping,[107–114] or atomic vacancies.[115] Defects such as Eu-O vacancies can cause volume expansion and structural distortions, weakening the antiferromagnetic Eu-Ti-Eu interaction and introducing a ferromagnetic Eu-O-Eu interaction.[115] Eu-O vacancies can be intentionally created using processes consisting of the growth of material by PLD and followed by a post-annealing treatment. ETO can be doped by many elements: for instance, La[107] and Gd[108] for the substitution at the Eu-site, or Nb,[109] Al,[110,111] Ga,[114] Sc,[112] and B[113] at the Ti-site. $SrRuO_3$ (SRO) is another well-known ferromagnetic material with a strong transition from paramagnetic to ferromagnetic behavior at a T_C of 160 K.[116] The ferromagnetic and metallic characteristics of SRO originate from the hybridization between the Ru 4*d* orbitals and the O 2*p* orbitals. To optimize the magnetic properties of SRO, controlling the growth conditions is crucial to minimize the vacancies of Sr, Ru, and O. Indeed, missing Ru and O atoms can hinder the movement of charge across Ru-O-Ru bonds, whereas missing Sr., atoms can cause local changes in the structure that affect the connection between Ru and O. Both situations can lead to a lowered T_C, so defects in SRO compromise its magnetic performance.[117]

4. Line and planar defects

Structural defects have shown intriguing electronic and magnetic landscapes in diluted magnetic semiconductor and non-magnetic materials,[118,119] unveiling the potential for utilizing "*dislocation* or *grain boundary technology*" to tune the magnetic properties of materials.[16–18] These defects can be classified into one-dimensional line

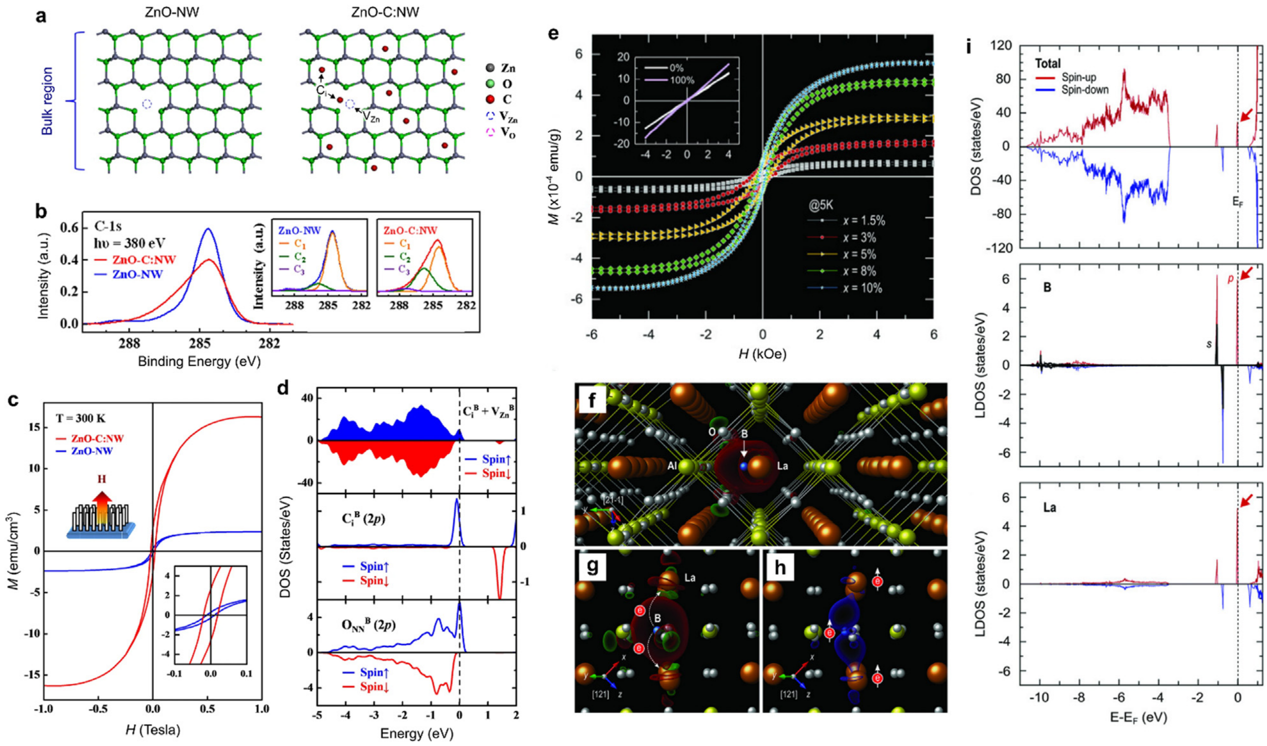

FIG. 4. (a) 2D atomic structure of ZnO-nanowire (NW) (left) and ZnO-C_i:NW (right). (b) x-ray photoelectron spectroscopy C 1*s* core level spectra for the ZnO-NW and ZnO-C_i:NW. The inset shows the deconvoluted components for the core level spectra: C_1, C_2, and C_3 are C=C, C–O, and C=O, respectively. (c) RT out-of-plane *M-H* curves of the ZnO-NW and ZnO-C_i:NW. (d) Calculated total density of state (DOS) (uppermost panel) and local DOS of carbon interstitial-Zn vacancy complex ($C_i + V_{Zn}$). The middle and lower panels show the 2*p* states of C_i and four nearest neighbor O atoms, respectively.[47] (e) 5 K *M-H* curves of the ferromagnetic LABO composite samples as a function of LBO composition, *x*. The inset exhibits the *M-H* curves of the paramagnetic undoped LAO and LBO. (f), (g) The charge density difference of a relaxed LAO supercell with a B_i (≈0.8 at. %), projected along the ⟨21-1⟩$_R$ (f) and ⟨121⟩$_R$ (g) zone axes. (h) The spin charge imbalance from the spin polarization states of the B_i:LAO supercell projected along the ⟨121⟩$_R$ zone axis. (i) The total DOS and the spin-resolved local DOS of the B_i:LAO supercell. The middle and lower panels show the *s*- and *p*-projected spin-resolved local DOS (LDOS) of B_i and the *d*-projected LDOS of the nearest neighboring La atoms, respectively.[37]

defects (e.g., edge and screw dislocations) and two-dimensional planar defects (e.g., grain boundaries, twin boundaries, and stacking faults), both of which can significantly influence the magnetic behavior of the material. Since such structural imperfections break local symmetry, alter the electronic structure, or introduce unpaired spins in oxide crystals, the presence of these defects often results in localized magnetism, spin-polarized states, or even long-range magnetic ordering, depending on the material and the nature of the defects.

In solid-state materials, dislocations are topologically extended defects that alter composition, strain fields, and charge over various scales. These line defects in oxides are formed with broken atomic bonds (dangling bonds), which create localized electronic states. These states can accommodate unpaired electrons and generate localized magnetic moments around the dislocation cores. The presence of uncompensated spins at the dislocation cores caused by the local symmetry change often results in ferromagnetic dislocations.[23] Additionally, since the dislocations act as effective charge (electrons or holes) trapping centers, the trapped charges can be spin-polarized, which leads to the emergence of localized magnetic order along the dislocations.[120,121] In some cases, the strain fields surrounding dislocations distort the bonding and electron density in the oxide lattices.[122,123] The defect-associated distortion can further alter the distribution of charge and spins, as well as the exchange interactions between localized spins, thereby modulating the magnetic response/coupling at or near the dislocations. The impact of such line defects has been demonstrated in various oxide materials such as TiO_2, ZnO, NiO, and $BiFeO_3$,[19–23] which can significantly modify their electronic and magnetic properties, e.g., a magnetic transition from AFM to FM at dislocation cores and RT-FM, as is shown for NiO in Figs. 5(a)–5(c).[23] More recently, such a magnetic ordering was visualized along the dislocation lines in oxygen-deficient or metal-doped $SrTiO_3$ single crystals subjected to large plastic deformation using scanning SQUID, as shown in Figs. 5(d) and 5(e).[119]

Similarly, planar defects, such as grain boundaries, have a more extensive impact on the crystal structure compared to line defects, as they extend over a larger area. These defect-rich regions energetically accumulate point defects (e.g., V_O and V_C), creating a local defect density of states. Such states act as sources of unpaired electrons (or holes), enabling the formation of a net magnetic moment and/or altering the magnetic exchange interactions. Furthermore, the presence of extended structural defects often appears to correlate with the emergence of a long-range FM order with a high T_C, as observed in diluted magnetic metal oxide nanostructures and polycrystalline oxide films. Grain boundaries serve as active sites for the preferential

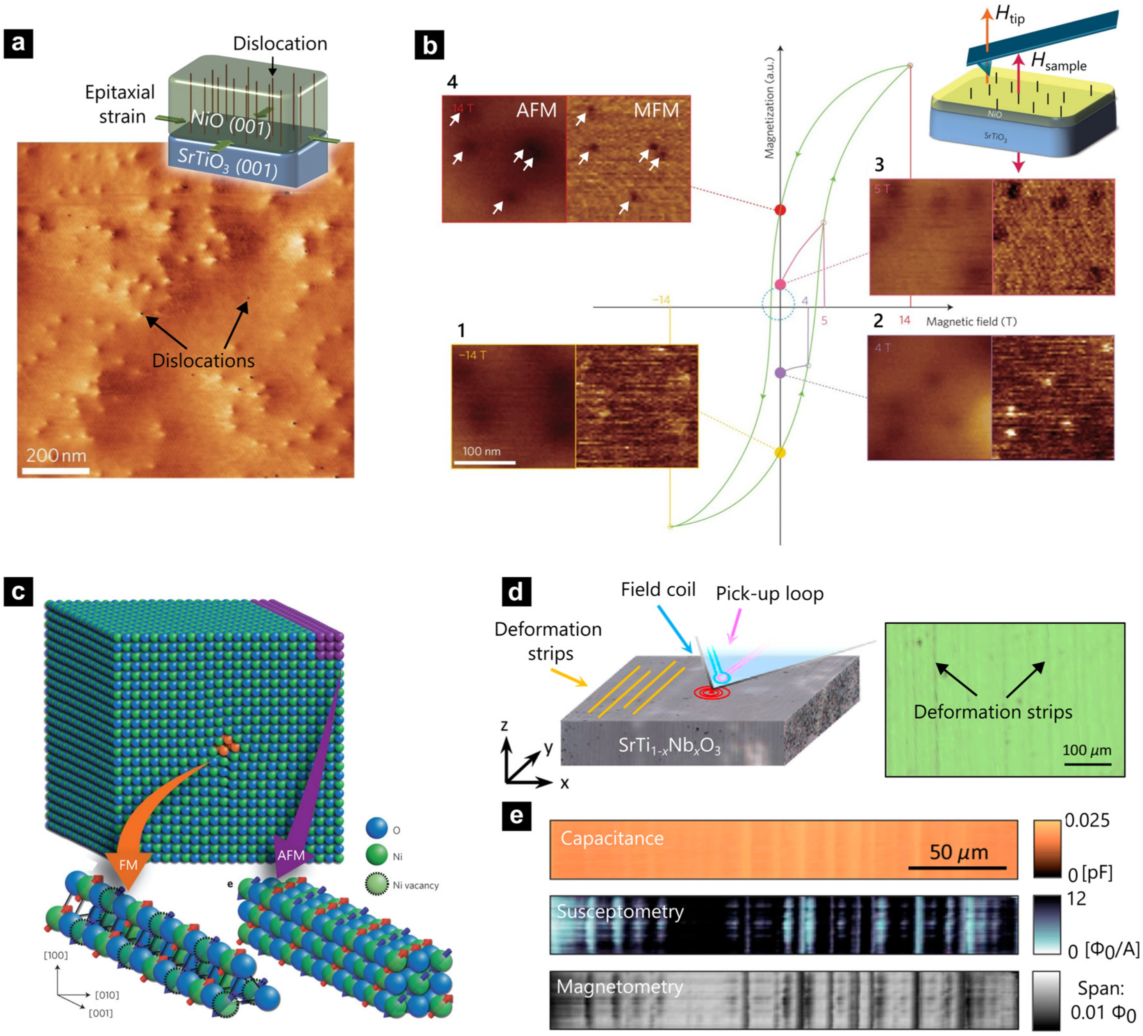

FIG. 5. (a) Dislocations into the NiO thin film under epitaxial strain show repulsive interaction in magnetic force microscopy (MFM).[23] (b) AFM and MFM images taken after applying magnetic field of −14 T (1), 4 T (2), 5 T (3) and 14 T (4) to the NiO thin film. The AFM and MFM measurements themselves were done under zero magnetic field.[23] (c) Atomistic model of the dislocation cores in NiO, arrows on the atoms show spin direction. Dislocations cores can possess ferromagnetic ordering in contrast to antiferromagnetic bulk.[23] (d) Schematic of scanning contact SQUID on dislocation walls in Nb doped $SrTiO_3$. The deformation stripes are visible under optical microscopy.[119] (e) Scanning SQUID images for capacitive surface sensing, susceptibility and spontaneous magnetization with magnetic stripe direction coinciding with optically visible deformed stripes.[119]

segregation of intrinsic defects and impurities observed in various oxide materials such as CeO_2,[121,124,125] Al_2O_3,[126] MgO,[124,127–129] and ZnO,[130,131] enabling the generation of an RT-FM.[125,132,133] Coey *et al.*[134] reported that a high-temperature FM in Mn (5%)-doped indium tin oxide (ITO) films is attributed predominantly to the role of grain boundaries. The FM originates from a "grain boundary foam," with an FM ordering confined to only a small fraction of the film volume. The remaining material stays magnetically inactive, underscoring the significance of localized defect regions in governing the magnetic properties. To understand the observed high-temperature FM, a charge transfer Stoner model was proposed, which involves spontaneous spin-splitting of uncorrelated electrons in narrow electronic bands. The unpaired electrons contributing to FM should be fully accompanied within the high-temperature FM phase, facilitated by defect segregation at energetically favorable sites (e.g., grain boundaries, surface states, or planar interfaces).[125] In the case of CeO_2, 4*f* electrons (associated with Ce^{3+}) and hydrogenic electron reservoirs (electrons trapped at V_O sites) could interact with each other, and electrons are transferred from Ce to V_O sites or vice versa to gain energy for the spin-splitting of the defect band. Such a charge-transfer FM was also observed in indium oxide (In_2O_3) with mixed-valence dopant cations (e.g., Mn^{2+}/Mn^{3+}) showing charge transfer between dopant ions and the local density of states associated with grain boundaries, see Figs. 6(a) and 6(c). This leads to Stoner-like splitting of the defect band and the resultant formation of a net magnetic moment,[135] see Figs. 6(d) and 6(f). Note that, in this model, the transition metal cation

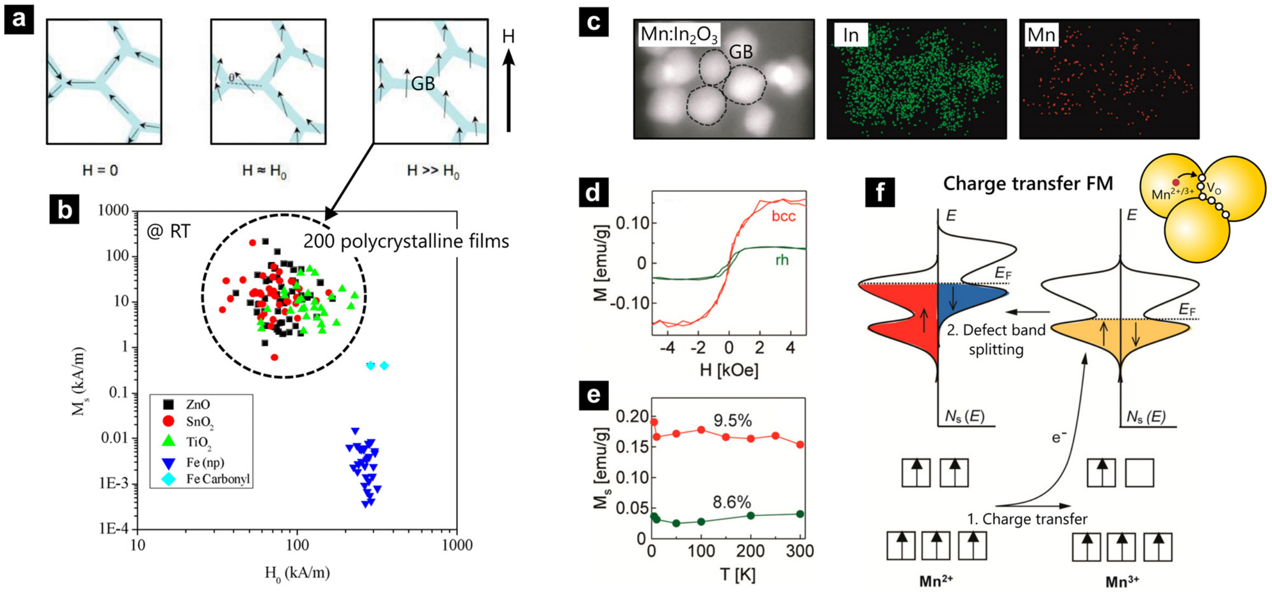

FIG. 6. (a) Schematic magnetization process where the magnetization is confined to the grain boundaries under an increasing applied field H. (b) Plot of sample saturation magnetization (M_s) vs switching field (H_0) for a wide range of anhysteretic ferromagnetic films.[134] (c) STEM image with corresponding EDX maps for an ensemble of 9.5% Mn: bbc-In_2O_3 nanocrystal (NC). (d) Magnetic hysteresis loop at 300 K for 9.5% Mn:bbc-In_2O_3 and 8.6% Mn:rh-In_2O_3 NC films. bbc and rh represent body centered cubic and rhombohedral structures, respectively. (e) Temperature dependence of the saturation magnetization for Mn:rh-In_2O_3 NC films. (f) Schematic of proposed charge-transfer ferromagnetism in NC dilute magnetic oxide. This involves electron transfer from Mn^{2+} to the local density of states associated with the interfacial structural defects, which raises the Fermi level in N_s and causes Stoner splitting of the defect band.[135]

dopants do not participate in the magnetic exchange interactions and, therefore, do not contribute a source for the magnetic moment of the system. Instead, their role is to facilitate the charge transfer process. Based on this, an intriguing aspect involves controlling the orientation of extended structural defects (e.g., grain boundary angle and the alignment of vertical boundaries) to generate strain fields in the surrounding host lattices along a certain crystallographic axis.[121,136,137]

Magnetic anisotropy in thin films arises from the interplay of competing factors, including magnetic crystalline anisotropy, strain anisotropy, shape anisotropy, and interface exchange anisotropy. In most FM multilayers, the magnetic easy axis lies within the in-plane of the substrate, a phenomenon known as shape anisotropy. This effect is driven by the size and shape of the substrate, which causes the magnetization to align either parallel to the in-plane of the layer or it can be along the length of needle-shaped nanoparticles, dots, or wires. In planar films, perpendicular magnetic anisotropy emerges from symmetry breaking at FM-nonmagnetic (NM) surfaces and interfaces, and when sufficiently strong, it can dominate the material's magnetic properties. Developing materials with perpendicular magnetic anisotropy is of great technological importance for downscaling storage cell size with superior thermal stability and thus has been an active area of research for decades, particularly for electronic applications such as data storage, high-density spintronic memory, and logic devices.[24,138,139] This underscores the potential of structural defect engineering in tailoring and controlling anisotropic magnetic properties. Specifically, controlled strain fields introduced by the engineering of out-of-plane (i.e., the film growth direction) structural defects can induce long-range spin alignment along the out-of-plane direction, promoting perpendicular magnetic anisotropy. The strain-induced effects modify the local electronic structures and spin–orbit coupling, which are critical for the emergence of magnetic anisotropy, often leading to a preferred magnetic easy axis along the boundary orientation of extended structural defects. Such strain field-driven magnetic anisotropy is particularly evident in highly textured films and vertically aligned nanostructured films, where atomically imperfect grain boundaries or vertically aligned interface amplify strain effects.[140–143] The orientation and density of these defects can be precisely engineered through film growth techniques such as pulsed laser deposition[42,144] and sputtering,[145–147] offering a tunable platform for anisotropic magnetic behavior. For instance, vertically aligned nanostructure systems comprising oxide matrices embedded with vertically aligned nanocolumns have shown an interesting platform for controlling magnetic anisotropy due to the interplay between vertical interface, defect, and magnetoelastic coupling. This is further discussed in Sec. II C. Beyond conventional magnetic materials, this phenomenon also provides opportunities in nonmagnetic oxides, where defect engineering can induce unexpected preferential magnetic orderings through strain-mediated spin polarization. Consequently, controlling the orientation of extended structural defects could serve as an effective strategy for designing materials with highly tunable and uniaxial magnetic properties.

B. Defect engineering by ion irradiation

In addition to defect engineering by controlling the growth condition, defects in crystalline materials can also be introduced by energetic ion beams. The most well-known example is ion implantation for doping semiconductors. In this process, implanted impurities, essentially defects in semiconductors, provide free carriers, thereby leading to control over electrical properties. Ion implantation has been maturely developed in the last several decades for micro- and nano-electronics industries. Here, we briefly discuss defect engineering by ion beam for oxide films, where the intrinsic defects, such as interstitials and vacancies, contribute to the magnetic modification.

The energetic ions injected into matter undergo collisions with the target atoms. Through a binary collision approximation, the interaction with the electrons and the nucleus is treated independently, referred to as electronic and nuclear stopping, respectively. The interaction with electrons will induce excitation and ionization of atoms in the host material. At low energy-density deposition, this process will not create atomic displacements. However, in the case of swift heavy ion irradiation, the high-density electronic excitation can deliver a significant energy payload to the host material lattice via electron-photon interactions. Per the thermal spike model, a narrow cylindrical zone of approximately 10 nm around the ion tracks undergoes a temperature surge, often surpassing the melting point of irradiated materials.[148] This temperature escalation is swiftly succeeded by rapid thermal quenching ($\sim 10^{14}$ K/s), triggering nonequilibrium thermodynamic reactions that generate point defects such as vacancies and interstitials. Nuclear stopping involves elastic collisions of ions with nuclei in the target and leads to atomic displacements, creating defects. The threshold displacement energy, E_D, is a critical factor in gauging the extent of lattice damage. It represents the minimum kinetic energy required to move an atom from its designated lattice position, forming a stable Frenkel pair. E_D is a material-dependent parameter, but mostly in a few tens eV range. The displaced atom (recoil atom) and the primary ion often possess adequate energy to displace additional atoms from their lattice positions, initiating a displacement cascade. This sequence persists until both the primary ion and all recoil atoms decelerate to kinetic energies below E_D, ultimately coming to a stop. As a consequence, the density and distribution of defects heavily rely on factors such as ion type, energy, and sample composition. They can be calculated through simulation via the stopping and range of ions in matter (SRIM) code.[149] Figure 7(a) shows an example of defect distribution in TiO_2 upon irradiation by O ions with different energy and fluence. The defect concentration and depth distribution can be well controlled by varying ion fluence and energy. Applying proper lithograph, one can also create diverse lateral patterns that are well-done for micro-electronics. It's important to highlight that SRIM does not consider dynamic defect annealing or the crystalline structure. Therefore, the defect concentration calculated by SRIM is a kind of upper limit.

As a wide bandgap semiconductor, TiO_2 was proposed as a candidate for dilute magnetic semiconductors by doping with transition metals. As a by-product, defect-induced magnetism was observed. Zhou *et al.*[151] used O ions to create defects, and the aim was not to introduce other foreign elements.[150] The authors demonstrated the induction of ferromagnetism in pure TiO_2 single crystals after ion irradiation, as shown in Fig. 7(b). Through a combination of x-ray diffraction, Raman scattering, and electron-spin resonance spectroscopy, the authors pinpointed a defect complex—specifically, the presence of Ti^{3+} ions occupying substitutional sites alongside oxygen vacancies—in the irradiated TiO_2. This defect complex triggers a distinct Raman mode, indicating a local (TiO_{6-x}) stretching effect. The investigation reveals that these Ti^{3+} ions, possessing unpaired 3*d* electrons, generate the localized magnetic moments observed. Later, many papers were published to reproduce the results.[151–154] Particularly, Stiller *et al.*[153] used low-energy Ar ion irradiation to anatase TiO_2 films and generated a thin (around 10 nm) ferromagnetic surface layer. They used elemental selective x-ray magnetic circular dichroism (XMCD) to understand the origin of the observed magnetism. It is revealed that a Ti band is spin-polarized. Together with density functional theory calculations, they suggested that Ti vacancy-interstitial pairs, where a Ti dangling bond acts as a defect forming TiO_5, are responsible for the magnetic order. On the other hand, Thakur *et al.*[151] measured the

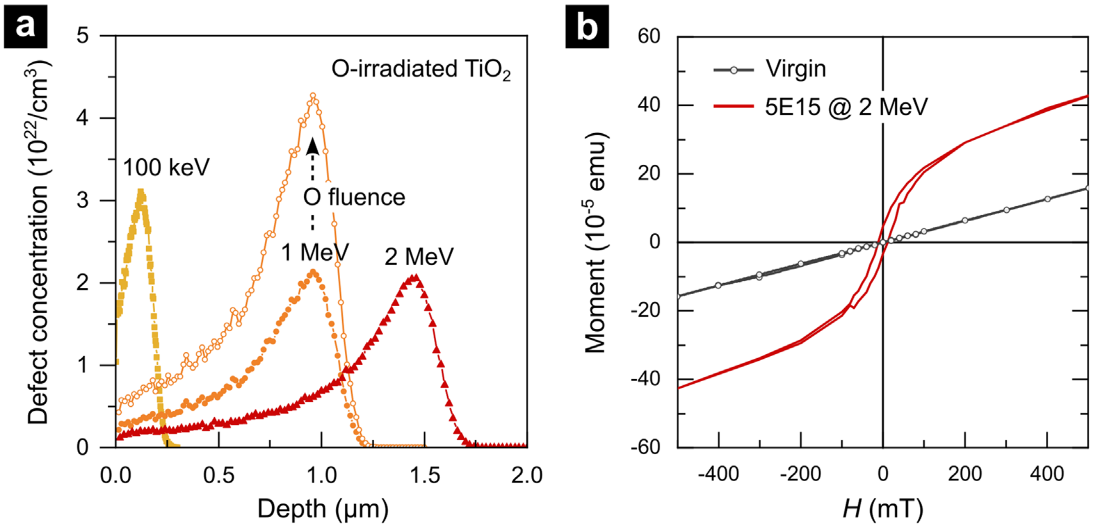

FIG. 7. (a) SRIM simulation of defect depth profile in TiO_2 irradiated by O ions with different energies (100 keV, 1 MeV, and 2 MeV) at the fluence of 1×10^{15} cm^{-2}. The open circle is for the fluence of 2×10^{15} cm^{-2}. One can see the correlation between the defect concentration and ion fluence, between the depth distribution and ion energy. (b) Magnetic moments measured at 300 K as a function of magnetic field for rutile TiO_2 crystals before and after irradiation. The O-irradiation was done with 2 MeV to the fluence of 5×10^{15}/cm^2. Inset: the low-field part of the loop for the irradiated sample.[150]

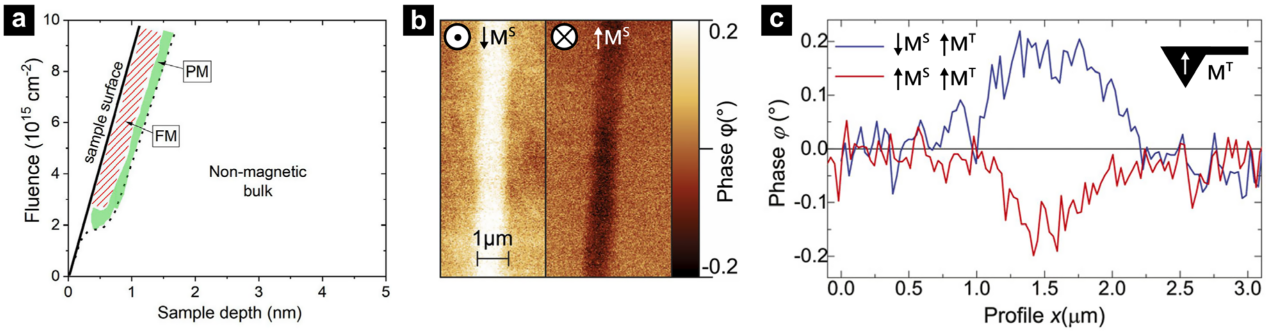

FIG. 8. (a) Semiquantitative magnetic phase diagram (fluence vs sample depth) for a TiO_2 anatase sample irradiated with Ar^+ ions of 200 eV energy. The straight line denotes the position of the sample surface, which shifts due to the sputtering. The red region is the FM region, and the green is a paramagnetic (PM) region. The dotted line represents roughly the transition region between a PM and a non-magnetic region, where the mean number of defects created by the irradiation is negligible. The dotted line can be considered the penetration depth of the irradiated ions. (b) Magnetic force microscopy measurements with the sample and tip magnetization (left) antiparallel and (right) parallel to each other. A clear phase shift was observed for two different configurations. (c) The corresponding line scans.[154]

magnetic polarization of the O-2*p* and Ti-3*d* orbitals in ion-irradiated anatase TiO_2 films. They suggested a sizeable coupling between the unquenched orbital moment within the O-2*p* shell and the neighboring Ti-3*d* moments, leading to the observed ferromagnetism.

By applying the standard lithography process, the TiO_2 film was covered with a resist, and electron beam lithography was used to prepare the mask. Ar ions were implanted through the mask and produced a stripe-like defective area with a width of around 750 nm.[154] Magnetic force microscopy (MFM) was used to measure the magnetic stray fields of the locally pattern regions, as shown in Fig. 8(a). The sample was magnetized in either an antiparallel or parallel [Figs. 8(b) and 8(c)] orientation concerning the MFM tip's magnetization direction. The observed phase shift in the MFM signal correlates well with the magnetization direction, consistent with expectations for a pinned ferromagnetic signal. Therefore, ion irradiation and proper lithography can create laterally patterned ferromagnetic areas in oxide films. ZnO is another well-known wide bandgap semiconductor. Different from TiO_2, in ZnO, it is unlike to have unpaired 3*d* electrons. Many papers showed defect-induced ferromagnetism in ZnO films or nanowires via ion irradiation.[155–159] Zn and O vacancies were proposed as the origin of the observed ferromagnetism. In the work by Lorite *et al.*,[160] a clear XMCD signal was observed at the O *K*-edge absorption. The authors suggested the ferromagnetism is due to the O-2*p* spin polarization induced by the proximity to zinc vacancies.

Defect-induced magnetism was also reported for CeO_2 via ion irradiation.[160–162] In the work by Shimizu *et al.*,[161] polycrystalline CeO_2 was irradiated by 200 MeV Xe ions at different fluence. Ferromagnetism was observed at room temperature, depending on the ion fluence. Various experimental results from x-ray diffraction and x-ray photoemission spectroscopy revealed the appearance of V_O after irradiation. In this case, V_O were created due to the high-density electronic excitation induced by 200 MeV Xe ions. This process induces a shift in the valence state of Ce atoms from 4+ to 3+, thereby localizing a 4*f* electron at each Ce^{3+} atom near the oxygen vacancies, maintaining charge balance. The authors suggested the likelihood of ferromagnetic interactions between 4*f* electrons situated on Ce^{3+} atoms within ion-irradiated CeO_2. Magneto-transport measurements were also performed to characterize the interaction between the defect-induced magnetic moment and the free carriers in oxides. One example is the negative magnetoresistance observed in ion-irradiated ZnO microwires.[163] It was attributed to spin-dependent scattering. The negative magnetoresistance also shows anisotropy depending on the current and magnetic field orientation, similar to the normal ferromagnetic systems. By applying lithography, Botsch *et al.*[165] prepared heterostructures with alternative magnetic and nonmagnetic regions along ZnO microwires by low-energy ion implantation. The observed magnetoresistance can be well explained by considering spin-polarized transport through a potential barrier acting as a minority spin filter. However, to our knowledge, there is no anomalous Hall effect, another fingerprint of ferromagnetic materials, reported in defect-induced magnetic oxides.

We have shown ion irradiation as a powerful tool to generate defect-induced magnetism in diverse non-magnetic materials. Yet, the strength of this approach lies in its versatile applicability, irrespective of the materials being processed, and its seamless integration potential with other techniques, such as lithography. The latter compatibility enables the creation of diverse lateral magnetic patterns. Furthermore, once the conceptual principle is approved, ion beam processing can be readily implemented at an industrial production level. A more comprehensive review of defect engineering by ion beam for oxide materials was given by Esquinazi *et al.*[6] However, a concrete picture of the magnetic coupling in defective oxides is still under discussion. One puzzle is that the induced magnetization is often weak despite the irradiation occurring in a bulk volume. Magnetization often depends on the ion fluence: the induced magnetization first increases with ion fluence, then decreases at large ion-fluence.[150,161] It is presumably attributed to the dilemma: defects are needed, but a proper crystalline structure must be kept. However, the Curie temperature does not depend on the ion fluences, i.e., the concentration of defects. As a sharp contrast, the well-known dilute magnetic semiconductors, e.g., Mn-doped GaAs, show a clear correlation between the magnetization, Curie temperature, and Mn concentration.[164] Such a correlation is missing in defect-induced magnetic oxides. One interpretation could be as follows. Although ion irradiation induces defects throughout a certain depth, it is probably only the surface or interface where the defect-induced local moments can develop ferromagnetic coupling.[154,165] From various experimental evidence, Stiller and Esquinazi suggested that the ferromagnetism in low-energy ion irradiated TiO_2

films only develops at the surface.[154] It shows a 2D magnetic nature with a perpendicular anisotropy.

In addition to inducing magnetism in non-magnetic oxides, ion irradiation was also used to tailor ferromagnetic oxide films. One of the prominent effects is the lattice expansion along the normal direction of the film, which consequently leads to enhanced tetragonality. This symmetry breaking can result in radical changes in the magnetic properties. In LSMO, the T_C is strongly decreased and in SRO, one sees the topological Hall effect.[166,167] A key limitation in using ion beams for defect generation is the inability to selectively produce specific types of defects. In elemental crystalline materials, ion irradiation creates vacancies and interstitials simultaneously. When it comes to compound semiconductors, ion irradiation often results in a range of defects, such as vacancies, interstitials from each element in the compound, and antisites, without the ability to target any one type specifically. However, this limitation can be mitigated by considering the thermal dynamics of these various defects. For instance, certain unwanted defects can be eliminated through mild post-irradiation annealing while preserving the functionally beneficial defects.

C. Strain induced magnetism

Applying strain is one of the more common approaches to induce ferromagnetism in non-ferromagnetic oxides. The role of strain is to change the crystal symmetry to allow the emergence of ferromagnetism. The coherent straining of oxides can be readily achieved through thin film growth and is used extensively to engineer magnetism in a wide range of non-d^0 transition metal oxides. The source of strain can be the substrate,[58,133–136,141] V_O present in the film,[23,142–144] impurity phases,[145,146] and vertically aligned nanocomposites (VANs).[11]

The interplay between strain and magnetic properties is well-studied for manganites. In these oxides, the magnetism is based on the superexchange coupling of mixed valence states of Mn (Mn^{3+}– Mn^{4+}, specifically $3d^4$–$3d^3$). The parental compound $LaMnO_3$(*Pbnm*), an *A*-type anti-ferromagnetic with $3d^4$ manganese moments, is often co-doped with divalent cations to engineer mixed valence compounds with ferromagnetic behavior, such as LSMO.[168,169] However, by applying strain, $LaMnO_3$ can also be driven to a ferromagnetic state. For example, antiferromagnetic to ferromagnetic transition can be tuned by straining $LaMnO_3/SrMnO_3$ superlattices through growth on lattice-mismatched substrates.[170–173] The magnetic ordering in the $LaMnO_3$-based superlattice occurs at the strained interface.

Studies of the $LaMnO_3$/STO interface reveal complex behavior, which is still under debate. Some studies show the crucial role of interfacial charge transfer and the following Mn-O-Ti superexchange coupling in stabilizing Ti^{3+} ferromagnetism.[174] Other studies show that charge transfer solely occurs in the $LaMnO_3$ layer because of the presence of an internal electric field due to the polar interface, which results in Mn-mediated ferromagnetism upon exceeding a critical thickness (Fig. 9).[175,176] A rich interplay between strain and magnetic properties for polar non-d^0 oxides is visible in perovskite materials such as the manganites.

The model of mixed valence states coupled by superexchange is more complex for oxides such as LaCoO3 (LCO). At low temperatures, the Co^{3+} ion possesses a low spin configuration ($t_{2g}^6\ e_g^0$) with a d^0 ground state in a temperature range of 30–120 K. The Co^{3+} ion then transitions to a paramagnetic high spin configuration ($t_{2g}^4\ e_g^2$).[177] Ferromagnetic ordering in LCO can also be engineered through epitaxial strain, such as the PLD growth of LCO on (100) oriented $(LAO)_{0.3}(Sr_2AlTaO_6)_{0.7}$ which shows ferromagnetic (FM) order extending throughout the film with a T_c of 85 K.[178] Various other substrates have been used to engineer ferromagnetic ordering in LCO.[77,179,180] By comparing different crystallographic orientations of epitaxial LCO film grown on the (100)-, (110)-, and (111)-oriented STO substrates, it has been found that the ferromagnetism of LCO films is particularly enhanced with the (110) orientation (out-of-plane direction), leading to an increase in T_c up to 90 K.[181] Enhanced magnetism reduces crystal field splitting and enhances Co-O charge transfer compared to growth with (111) or (100) crystallographic orientation. Modification of ferromagnetism through oxygen vacancies in LCO thin films remains, to this day, a controversial topic despite decades of research. Contrasted vertical stripes were recorded by Choi *et al.*[31] using *Z* (atomic number)-contrast scanning transmission electron microscopy (STEM). The number of stripes varies with the degree of tensile strain. According to Choi and colleagues, these stripes are modulation of the lattice caused by the formation of twin domains. Furthermore, they support that the origin of tensile-strain-induced ferromagnetism is only consequent of an epitaxial strain and its resultant atomic displacements as they deduce from x-ray absorption and optical conductivity measurements.[181] Vertical stripes were also reported by Biškup *et al.*[182] using STEM. However, electron-energy-loss spectroscopy (EELS) data shows that the observed stripes are O-deficient regions, proving the presence of V_O.

Furthermore, Biškup *et al.*,[182] demonstrate that the tensile-strained LCO film relaxes by producing V_O superstructures and they link the superstructures to the induced-magnetism in LCO. The role of oxygen vacancies was confirmed by Zhang *et al.*,[183] which showed that the V_O ordering is parallel to the interface with the substrate under compressive strain. In contrast, under tensile strain, this ordering is vertical. The concentration and distribution of V_O are related to the value of the strain.[183] More recently, Li *et al.*[68] related the long-range ferromagnetic ordering in LCO to the combined effect of forming ordered V_O and the long-range order that suppressed CoO_6 octahedral rotation, weakening crystal-field splitting and promoting the Co high spin state. In addition to the role of V_O in maintaining magnetic order, various studies on LCO also attribute the ferromagnetism to interfacial strain at Co_3O_4 impurity phases, which is supported by the notion of increased ferromagnetism in polycrystalline LCO compared to a single crystalline LCO.[184,185] The true microscopic origin of strain-induced ferromagnetism in LCO is attributed to the strain induced by substrates, V_O and impurity phases.

In addition to tuning the magnetism through the in-plane strain, designing self-assembled film structures such as vertically aligned nanocomposites enables the induction of significant vertical strain which can effectively can tune the intrinsic magnetic properties of the film (Fig. 10).[11] For example, Lin *et al.*[186] reported that in ETO_{1-x}: $Eu_2O_3(EO)_x$ nanocomposite thin films, the out-of-plane strain of the films is increased up to +3.15% by an EO fraction of $x = 0.5$, while the in-plane strain remains constant. Thus, the vertical strain lowers the Eu-Ti-Eu bond angle (more than 1°) along the [111] direction, subsequently weakening the antiferromagnetic interaction [Fig. 10(e)]. The authors suggested that such a strain-mediated tetragonality leads to a switch in the dominant magnetic interaction from antiferromagnetism (between first and third NN Eu^{2+} ions via Ti 3*d* band) to ferromagnetism (with second NN Eu^{2+} ions). Additionally, in the case of

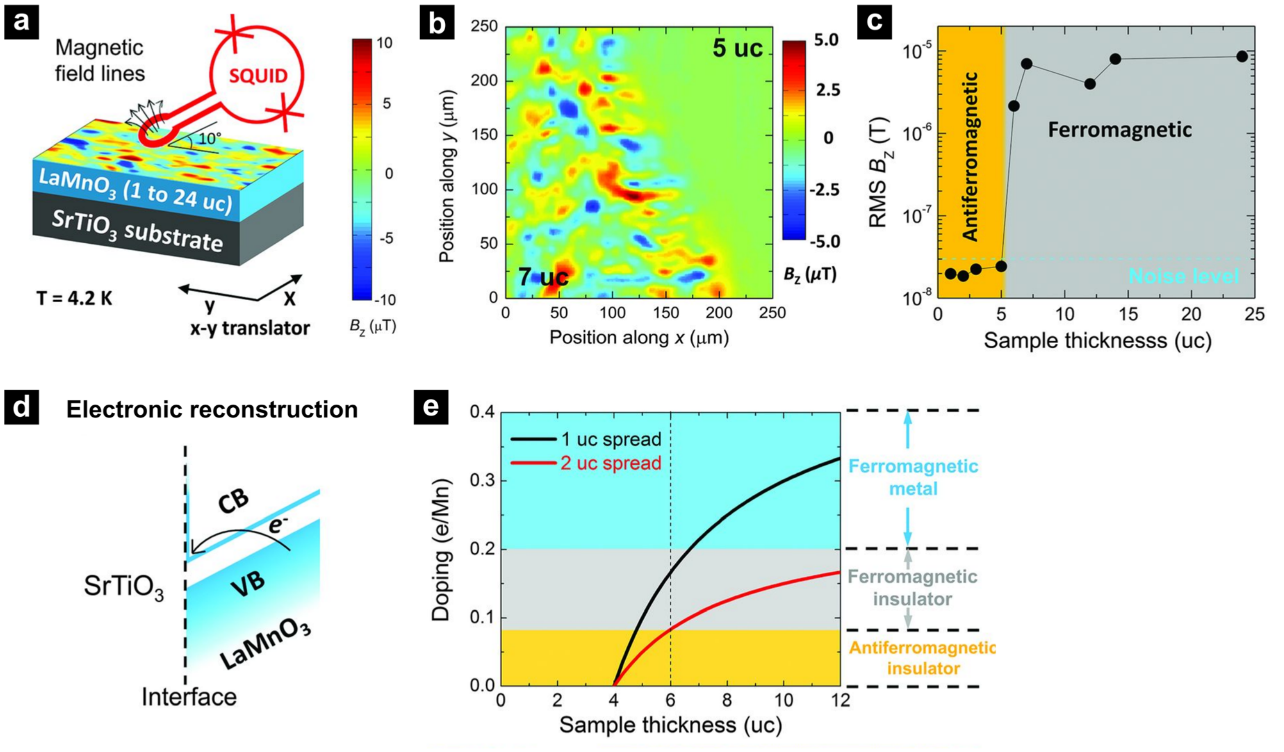

FIG. 9. (a) Schematic for imaging the local magnetic stray field distribution of the LMO films, captured by scanning superconducting quantum interference device (SQUID) microscopy with the pickup loop. (b) Abrupt appearance of in-plane magnetic field distribution when a 5 unit cell (UC)-thick (upper right area) and a 7 UC-thick (bottom left area) LMO films are compared. (c) A profile for the RMS local field amplitude (B_Z) of the LMO films as a function of thickness. From Wang *et al.*[175] (d) A sketch for the band diagram of electronic reconstruction at the LMO(100) and STO interface (CB:conduction band, VB:valence band). (e) Amount of charge transfer of the Mn site from the surface to the interfacial layer as function of LMO thickness. A ferromagnetic metal phase is formed with the LMO thickness of >6 UC.[175]

MgO:LSMO VAN system, it was found that the magnetic anisotropy of the host oxide matrix, i.e., ferromagnetic LSMO, can be tuned by controlling vertical strain.[187] The out-of-plane strain increases linearly with MgO volume (vertical interfacial area between MgO and LSMO) up to MgO volume of 10%. When the MgO volume exceeds 5%, the anisotropy of the LSMO is switched from the in-plane easy axis to the out-of-plane axis. MgO volumes exceeding 10% lead to increasing interfacial dislocation density such that the LSMO is no longer coherently strained. VANs can maximize strain tuning in both the in-plane and out-of-plane axis by utilizing 3D scaffold networks for example, LSMO:CeO$_2$ 3D-scaffold networks are used to strain tune the magnetoresistance to high value of 66% at 56 K.[31]

III. METHODS OF CHARACTERIZATION

This review focuses on recent advancements in the field of defect-induced symmetry breaking. Magnetic characterization of defect-induced magnetism becomes increasingly challenging as the system approaches the limits of dilute magnetism, approximately ~5 at. %.[188] In general, measurements, such as vibrating sample magnetometry (VSM) and superconducting quantum interference devices (SQUID), collect the magnetic properties across the entire sample volume for sensitivities down to 10^{-6} emu. However, for novel studies into weak, defect-induced magnetism, typical magnetic moments are on the order of 10^{-5} emu; these could also be possibly due to magnetic contamination, for example, a magnetite particle of radius 17 μm or a single monolayer of Fe on a $6 \times 6\,\text{mm}^2$ substrate.[46] Reliable measurements and studies will require a reproducible trend over a range of sample parameters with theoretical support. Ideally, the source and mechanism of the magnetism are clarified by additional magnetic characterization techniques addressing magnetism on the local and microscopic scale. An overview of common thin film magnetic measurement techniques is provided in Table I. The rich interplay of magnetic properties with all aspects of physics, such as electrical, structural, and optical properties, allows for many approaches for qualifying and quantifying the magnetic properties of materials. The list of measurement techniques provided in Table I is far from exhaustive; a more general and extensive overview can be found in the referenced literature, such as Christensen *et al.*[189] regarding microscopy techniques and more generally Coey *et al.*[191]

IV. INSIGHTS FROM FIRST PRINCIPLES CALCULATIONS

Ab initio (or first principles) calculations of oxide films and heterostructures within the density functional theory (DFT)[196] contribute to improve our understanding of the materials with specifically targeted functional properties. Presently, modern state-of-the-art DFT codes allow researchers to calculate important magnetic properties such as thermally excited magnetic fluctuations, magnons, various magnetic interactions, and critical magnetic-transition temperatures

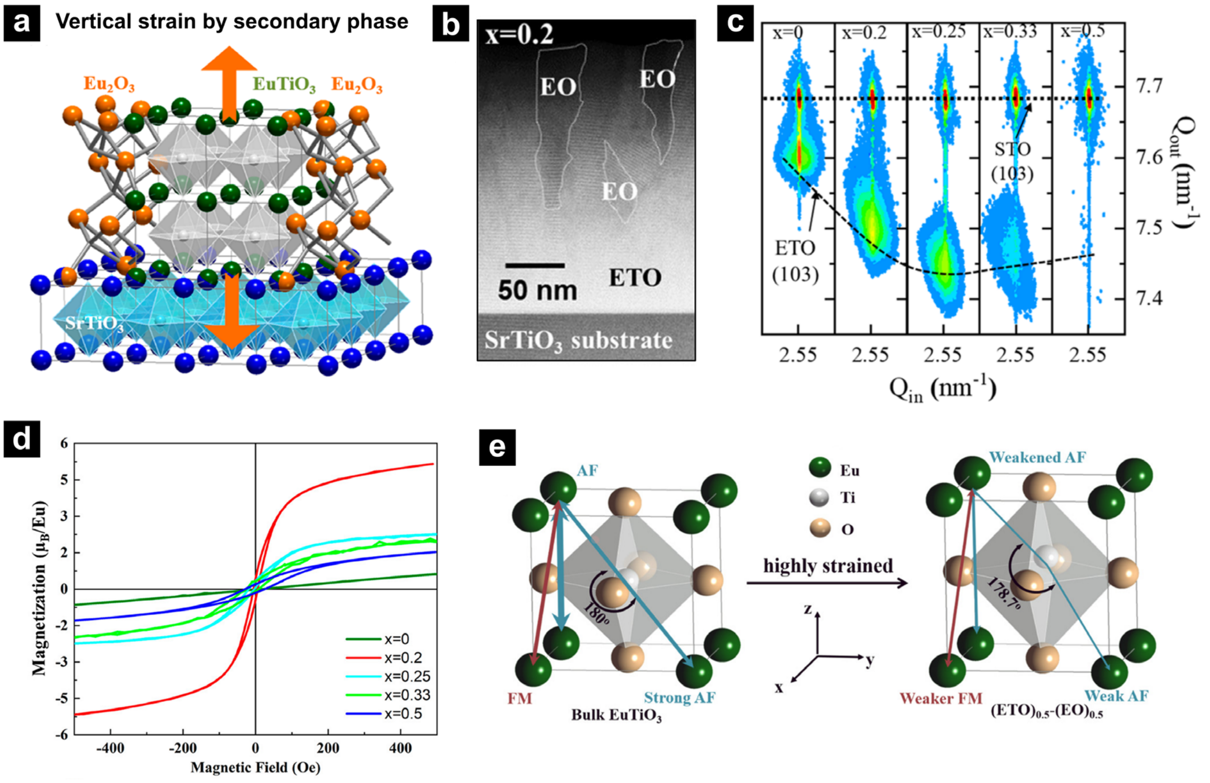

FIG. 10. (a) Vertical strain is induced in the $EuTiO_3$ (ETO) by the secondary Eu_2O_3(EO) phase. (b) Schematic for an $ETO_{0.8}$:$EO_{0.2}$ nanocomposite film structure on STO substrate and an HAADF-STEM image for the $ETO_{0.8}$:$EO_{0.2}$/STO sample. (c) Out-plane lattice expansion evolution for ETO_{1-x}:EO_x nanocomposite films ($x = 0$–0.5). (d) 2 K-magnetic hysteresis loops for the ETO_{1-x}:EO_x nanocomposite films ($x = 0$–0.5). (e) Schematic illustration for the alternation of magnetic interaction strength in ETO by a large vertical strain, which changes the Eu-Ti-Eu bond angle along the [111] direction.[186]

(T_c).[193,194] When spin–orbit coupling (SOC) is considered, it is possible to calculate magnetic anisotropy, non-collinear spin structures, and spin textures.[197,198] In addition, the broken inversion symmetry in oxide heterostructures lifts its spectral degeneracy that is widely used as the Rashba SOC effect.[199] Here, we review the recent and significant results of *ab initio* calculations for epitaxially grown perovskite films and heterostructures, in which point defects, strain, and interfacial chemistry induce magnetism:

i. **Diluted magnetic oxides:** Chronologically, the thin-film nonmagnetic oxides were the first widely debated oxide materials in the context of their induced magnetism and activation of improper magnetic phase transitions. The experimental findings of room-temperature FM in thin films of Co-doped TiO_2,[200] HfO_2,[201] and Cr-doped In_2O_3[202] stimulated a considerable interest in diluted oxides, which can become ferromagnetic when doped by the 3*d* metals. The magnetic properties of doped oxides, however, are heavily dependent on the structure and defects that complicate a whole picture. For example, $Zn_{1-x}Mn_xO$ is not ferromagnetic, although the theory predicts its possible appearance.[203] Another example is Mn-stabilized cubic ZrO_2. DFT anticipates a FM ordering,[204] which seems to be robust to oxygen vacancies up to 500 K. So far, however, the expectations of high T_C in Mn-stabilized zirconia have not been confirmed experimentally. In thin films of diluted magnetic oxides, a variety of factors, such as the sample preparation, relatively low solubility, and phase separation, continue to keep T_C far below room temperature. Due to computationally restricted supercell, DFT simulations usually overestimate the dopant concentration. Moreover, a regular dopant sublattice is unavoidably modeled due to periodic boundary conditions, which are far from reality and that may result in the high-T_C ferromagnetism.

ii. **LAO/STO:** To this end, a rich expertise has been built up on the quasi two-dimensional electron gas (*q*2DEG) emerging at the interface between two band insulating perovskites. The first-time *q*2DEG was detected beneath polar LAO epitaxially grown on the TiO_2-terminated STO(001) substrate.[25] Besides its room-temperature metallization, the *q*2DEG-LAO/STO also shows superconductivity,[205] gate-tunable Rashba SOC,[206] and magnetism. Early evidence of unexpected FM hysteresis were found in LAO/STO shortly after the discovery of *q*2DEG.[207,208] It seems that electronic reconstruction at LAO/STO is necessary, but it is insufficient for its FM. *Kalisky* et al.[209] proposed that the LAO/STO magnetism appears as a complexity where the population of interfacial carriers, disorder, and local strain intermix. As for the bare STO (001) surface, its high-temperature FM-like response has been discussed recently by Coey *et al.*[34] who suggested that a giant orbital paramagnetism could appear in

TABLE I. Overview of magnetic characterization methods, presenting descriptions of each technique and their sensitivity and spatial resolution.

Characterization techniques	Description	Sensitivity and resolution
Vibrating sample magnetometry (VSM)/superconducting quantum interference device (SQUID)[190,191]	VSM and SQUID are commonly used to measure the magnetic properties of both bulk and thin film samples. Magnetic properties such as susceptibility and hysteresis can be measured over a wide range of temperature and magnetic field.	Sensitivities for VSM and SQUID are respectively 10^{-6} emu and 10^{-8} emu. The measurement is performed over the entire sample volume.
Magnetic force microscopy (MFM)[189,191]	MFM is a form of atomic force microscopy (AFM), which probes qualitatively the surface topology and magnetization by magnetized AFM tips.	Sensitivity of 10^{-13} emu can be achieved with a spatial resolution of 20 nm.
Scanning-SQUID[189,192]	Currents, magnetic domains and magnetic defects can be imaged by scanning a sample surface using a SQUID loop. The detected signals are understood in terms of magnetic flux.	Sensitivity and spatial resolution compete for SQUID. Spatial resolution is possible from $\sim$50 nm to 10 mm with field noise of respectively 10^{-6} to 10^{-12} T/Hz$^{1/2}$
x-ray magnetic circular dichroism (XMCD)[191,192]	XMCD is a form of x-ray absorption spectroscopy (XAS) where a difference spectrum for a left and right circularly polarized x-rays is taken. Atomic element specific magnetic properties can be obtained through the probing of the core levels.	Spatial resolutions of $\sim 2\,\mu$m can be achieved with sensitivity capable of probing monolayers of magnetic atoms.
Magneto-optic Kerr Effect (MOKE)[191,193]	Magnetic domains can be imaged based on the optical Kerr effect, where the polarization of an incident linear light experiences changes in ellipticity and rotation upon reflection on a magnetized thin film, depending on its magnetization.	MOKE can reach optical resolution $<1\,\mu$m, in principle only limited by the Rayleigh criterion. Surface sensitivity is from a minimum of $\sim$2 UC to a maximum of $\sim$20 nm for ferri- and ferromagnetic materials.
Magnetic neutron diffraction[191,194,195]	Neutron scattering yields information about the spatial and directional ordering of nanoscale magnetic structures. Small-angle neutron scattering (SANS) and polarized neutron reflectometry (PNR) techniques are particularly effective for studying nanoscale spin textures (e.g., skyrmions and domain walls) and for measuring the depth-dependent magnetic variations (e.g., the strength and length scale of magnetism) in thin films, heterointerfaces, and multilayers.	In general, neutron diffraction techniques (SANS and PNR) allow resolving structure sizes on the order of 1–300 nm. PNR is a reflection geometry based technique with a surface sensitivity of up to a few tens of nm, well suited for ultra-thin films. SANS is operated in transmission geometry with a probing depth up to 1 μm.

coherent domains due to resonant interaction with zero-point fluctuations.[210] This scenario has also been used to explain the temperature-independent magnetization seen in ceria nanoparticles and nanoporous amorphous alumina.[132] In the lack of generally accepted theoretical explanation and using the bulk constituents only, the researchers are not able to reliably examine the *q*2DEG magnetism. Here, accurate DFT calculations are needed desperately. Until recently, all *ab initio* based explanations of the LAO/STO magnetism used the mechanism of electronic reconstruction emerging due to interfacial V_O.[211] Indeed, by placing one oxygen vacancy per two interfacial Ti, their oxidation states Ti^{3+}/Ti^{4+} can be simulated.[57] The V_O model, combined with the Hubbard parametrization of $\sim$5 eV applied on the 3*d* states of interfacial Ti, yields the magnetic double exchange interactions between Ti^{3+} and Ti^{4+}, leading to the coexistence of FM and *q*2DEG.[212] Obviously, FM correlations appear in heterostructures when LAO is simply replaced by magnetic insulator: $GdTiO_3$/STO,[213] $LaAl_{1-x}Mn_xO_3$/STO,[206] and EuO/STO.[214] Recently, it has been demonstrated that the introduction of ETO or LMO thin layer between LAO and STO induces there the spin-polarized *q*2DEG.[215] In the LAO/ETO/STO, as indicated by DFT,[215] the FM interactions are induced by the Eu^{2+} 4*f* magnetic moments. In fact, due to the broken inversion symmetry, the scenario of frustrated antiferromagnetism in the Mott-insulator thin overlayer grown on the band-insulator substrate should always result in a weakly FM interface. For the case of $LaTiO_3/KTaO_3$, such calculation has been reported.[216]

iii. **Cation-deficient oxide films:** In the STO thin films grown on STO(001), the magnetism can be induced and tuned by controlling the Ti vacancies and Ti-O vacancy pairs, as mentioned in the experimental section of this review.[8] The corresponding *ab initio* calculations show that each Ti vacancy in the STO overlayer induces 0.48 μ_B to the neighboring O and Ti. The O vacancy energetically tends to be paired with Ti vacancy that yields after relaxation 0.7 μ_B/pair.[8] The calculated magnetization

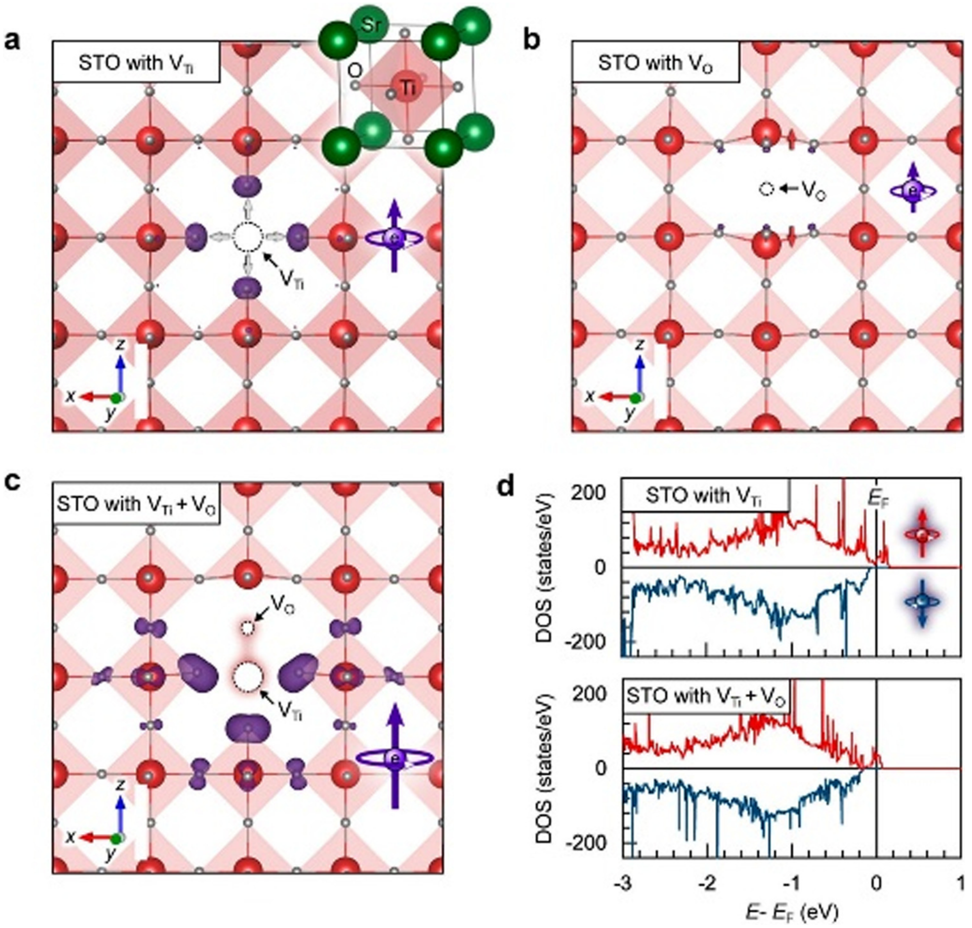

FIG. 11. Magnetization density of the ABO_3-perovksite STO structures, induced by different atomic vacant defects, a Ti vacancy V_{Ti} (a), an oxygen vacancy V_O (b), and a V_{Ti}-V_O pair (c). (d) Spin-polarized density of states of the STO with a V_{Ti} (upper panel) and with a V_{Ti}-V_O pair (lower panel).[8]

density and density of states is shown in Fig. 11. In the case of LAO/STO, there is a clear experimental evidence that the perovskite B-cation deficiency is crucial for the creation and control of interfacial magnetism.[12] To understand the reported magnetism the authors simulated from first principles an isolated Al (Ti) vacancy in tetragonally compressed LAO (cubic STO). Both B-site cation vacancies lead to spin polarization emerging mainly due to partially unsaturated p-orbitals of six nearest O atoms. This yields the total magnetization of about 0.9 μ_B and 0.5 μ_B per each Al and Ti vacancy, respectively.[12] Assuming the presence of aluminum vacancy near the LAO/STO interface, the subsequent antisite defect formation across the interface creates the total magnetization of $\sim$1 μ_B while the Ti substitute has itself the magnetic moment of about 0.5 μ_B.

iv. **Light impurities and efficient charge-to-spin conversion:** The n-doping of oxide overlayer in heterostructures by light impurities such as Li, Na, and B, can induce the q2DEG and, simultaneously, local spin polarization. For instance, the two-phase nanocomposite LABO thin films grown on STO (001) cause the coexistence of q2DEG and magnetic anisotropy associated with B interstitials in LAO. Simulations suggest that energetically unfavorable clustering limits the B doping in LABO by 3.2 at. % while B relax at the interstitial positions between La atoms, thus forming the La-B-La chains.[42] In a tetragonally compressed LAO that mimics the LAO/STO mismatch, the in-plane La-B-La chains expand, as compared to the out-of-plane chains. In this regime, together with significantly relaxed four nearest oxygens to each B, the in-plane La-B-La chain shows the La and B magnetic moments less than 0.02 μ_B, whereas each out-of-plane chain induces the magnetization up to 1 μ_B. Therefore, DFT confirms that the experimentally observed preferential magnetic order perpendicular to the LABO film layer.[42] The most recent *ab initio* studies suggest that when the initially insulating interface between LAO(111) and a solid-state electrolyte $LiNbO_3$ (LiNO) is doped by lithium[217] or by hydrogen,[218] the interface becomes metallic and weakly magnetic. The induced local magnetic moment and magnetization density due to lithium doping is shown in Fig. 12. Due to electric polarization in LiNO, the

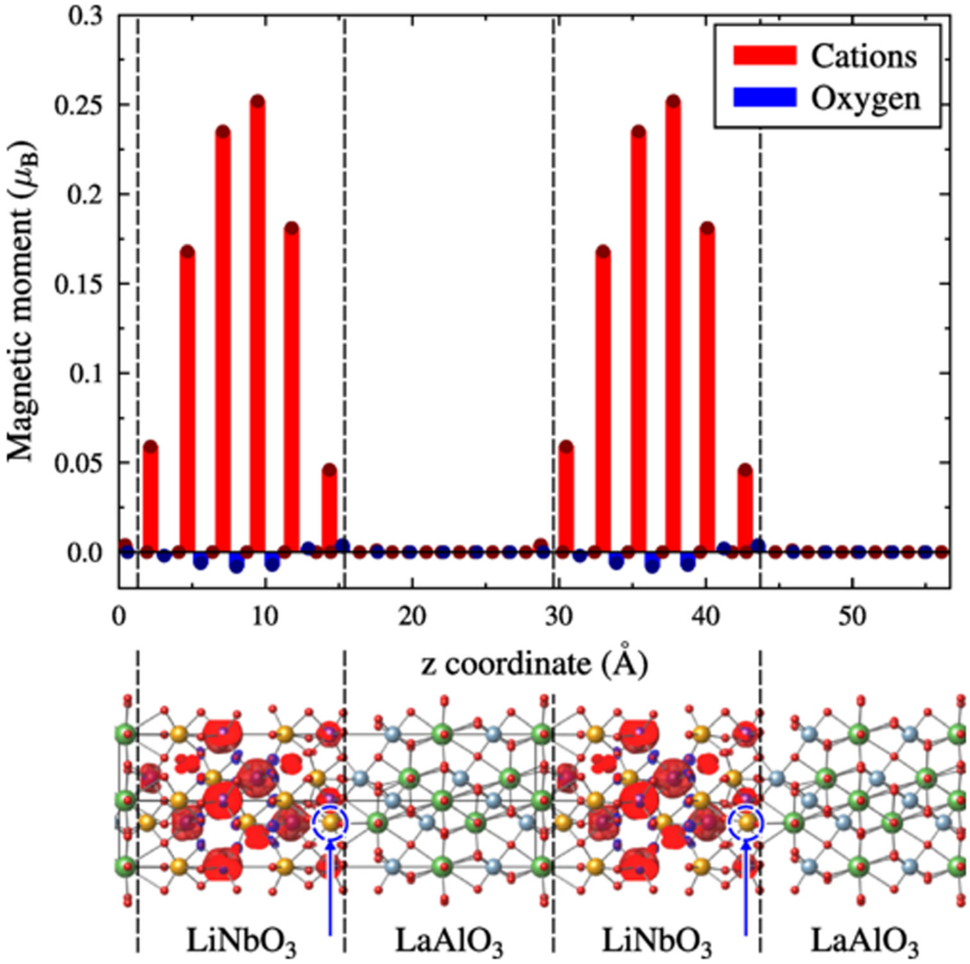

FIG. 12. The local magnetic moments induced in LaAlO$_3$/Li$_{1.17}$NbO$_3$ (top panel) and the side view of its magnetization density (low panel). The position of an excessive Li near the interface is marked by blue arrow and circle.[217]

dopant position at the Al-terminated LAO/LiNO interface is strongly preferable, while the *q*2DEG emerging there is spin-polarized. The calculated 1 μ_B-magnetization, which is induced in the LAO/LiNO by each light Li dopant, is distributed between the Nb species near the interface, within the spatial thickness of *q*2DEG. Moreover, the SOC provides there the non-collinear spin textures that are a promising basis for further spin-orbitronic implications and externally tunable *q*2DEG.

v. **Octahedral rotations and distortions in oxides:** The network formed by transition metal ions and O ions give rise to the wide range of properties of transition metal-based perovskite oxides. Typically, the electronic structure near the Fermi level is comprised by the B-site *d* orbitals and O *2p* orbitals. The overlap between these orbitals is sensitive to the B-O bond lengths, but also to the B-O-B angles. The strong sensitivity is due to the directional nature of the *d* and *2p* orbitals. Moreover, the electronic bandwidth is dependent on the orbital overlap. Hence, the crystal structure is directly connected to the effective correlation strength *U*/*W* (where *U* describes electron-electron interaction and *W* is the bandwidth). A strong correlation, *U*/*W*, can result in a Mott insulating phase.[219] Furthermore, the magnetic interaction is sensitive to the connectivity of the orbitals.[220] This is the reason why perovskite oxides can exhibit a wide range of electronic and magnetic phases with respect to structural distortions of the octahedral network. Perhaps even more intriguingly, the concept of inducing specific octahedral rotations or Jahn-Teller distortions *on demand* has been investigated.[221] Here, biaxial strain can be applied to stabilize/destabilize octahedral rotations. Moreover, it has been shown that octahedral rotations can propagate from one material to another, hence, new rotations might be available by combining perovskite oxides with different intrinsic rotations.[31,222] Manipulating the octahedral rotations through strain or proximity effects to alter the magnetic properties is a fascinating direction. Here, *ab initio* simulations have been crucial for guiding and explaining experiments, and we anticipate that further computational studies of the interaction between structural changes (such as rotations), strain and interfacing will help progress the understanding of how to control magnetism in oxides.

vi. **Role of strain and oxygen vacancies on magnetism in LSCO:** The family of $La_{1-x}Sr_xCoO_{3-\delta}$ (LSCO) shows rich electronic and magnetic phase diagrams, as discussed in the experimental sections. Upon doping with Sr, LSCO undergoes an insulating-metallic transition, accompanied with a transition from AFM to FM.[223] The introduction of Sr changes the oxidation state from Co^{3+} to Co^{4+}, which alters the exchange interaction, favoring FM ordering over AFM.[224] Interestingly, the FM state of epitaxial LSCO thin films can be destabilized by applying in-plane tensile strain (e.g., LSCO/STO).[223] Hence, the magnetic phase diagram is a function of both Sr content and strain. Zhang and Galli[31] further demonstrated using DFT + U that V_O is key to the electronic and magnetic properties of LSCO. They demonstrated a gradual transition from FM to fully AFM, when the parameter, δ, was tuned from 0 to 0.5. Furthermore, the magnitudes of the magnetic moments were enhanced upon oxygen depletion. Interestingly, they demonstrate that the role of V_O on the electronic structure is closely connected to lattice expansion, structural distortions, and magnetic ordering. It is therefore essential to allow all of these parameters to vary in simulations to understand the behavior of these oxides. Since both strain and oxygen vacancies are important for the magnetic structure, the question whether the magnetism in LSCO (and other oxides) can be further modulated by *combining* strain and vacancies is worth considering. They presented a systematic variation of the octahedral tilt angles with V_O which could be in competition (or enhanced) with rotations stabilized by factors such as V_O concentration and biaxial strain.[225]

It is evident that symmetry breaking—either due to point defects, e.g., vacancies or dopants, or from strain or heterostructures—notably modifies the magnetic structure of perovskite oxides. Since it can be challenging to control these parameters independently in experiments, *ab initio* calculations give much needed insights into *which* parameters are important, but also *how* said parameter modifies the magnetic mechanisms.

V. SUMMARY AND OUTLOOK

In this review, we comprehensively explore how defects such as vacancies, interstitials, and dopants in oxide materials influence magnetic properties, introducing the concept of defect-induced magnetism. This review discusses the challenges in creating and manipulating these defects at an atomic level and the theoretical complexities in understanding their impact on magnetism. The review highlights advanced experimental and theoretical approaches as keys to unraveling the role of defects in magnetism, suggesting potential technological applications in designing materials with specific magnetic properties.

Key areas for future development and potential breakthroughs include:

(1) *Advanced Material Design*: There is a growing necessity to create new materials with specific magnetic properties. This involves engineering defects within materials to fine-tune their properties and manipulate the defects in materials at the nanoscale, providing opportunities for innovative applications in more efficient transistors, advanced memory devices, and components for quantum computing.
(2) *Improved Theoretical Models*: Enhancing theoretical models, incorporating machine learning, is crucial for discovering new compounds and designing microstructures and magnetic defects. These models aim to provide a more accurate understanding of the interactions and mechanisms involved in defect-induced magnetism.
(3) *Enhanced Experimental Techniques*: Progress in experimental methods, such as advanced spectroscopy and high-resolution imaging, will enable in situ observation and manipulation of defects at the atomic level.
(4) *Defect Stability*: Research is likely to focus on improving the stability of defect-induced magnetic properties under various environmental conditions and temperatures, increasing the usability of these materials in practical applications.

ACKNOWLEDGMENTS

N.P. acknowledges the support of Novo Nordisk Foundation Challenge Programme 2021: Smart Nanomaterials for Applications in Life-science, BIOMAG (Grant No. NNF21OC0066526), the support from the ERC Advanced "NEXUS" (Grant No. 101054572), and the Danish Council for Independent Research Technology and Production Sciences for the DFF-Research Project 3 (Grant No. 00069B). D.-S.P. acknowledges the funding from Villum Fonden (SYMTEC, Grant No. 53078). S.Z. thanks the financial support from the German Research Foundation (No. ZH 225/10-1). V.E. and Y.W. acknowledge the Danish Council for Independent Research Technology and Production Sciences for the DFF- Research Project 2 (Grant No. 1032-00261B). A. E. acknowledges funding from the Fonds zur Förderung der Wissenschaftlichen Forschung (FWF) under Grant No. I 5384.

AUTHOR DECLARATIONS

Conflict of Interest

The authors have no conflicts to disclose.

Author Contributions

Eric Brand: Conceptualization (equal); Project administration (equal); Writing – original draft (equal); Writing – review & editing (equal). **Victor Rosendal:** Writing – original draft (equal); Writing – review & editing (equal). **Yichen Wu:** Writing – original draft (equal); Writing – review & editing (equal). **Thomas Tran:** Writing – original draft (equal); Writing – review & editing (equal). **Alessandro Palliotto:** Writing – original draft (equal); Writing – review & editing (equal). **Igor V. Maznichenko:** Writing – original draft (equal); Writing – review & editing (equal). **Sergey Ostanin:** Writing – original draft (equal); Writing – review & editing (equal). **Vincenzo Esposito:** Writing – original draft (equal); Writing – review & editing (equal). **Arthur Ernst:** Writing – original draft (equal); Writing – review & editing (equal). **Shengqiang Zhou:** Writing – original draft (equal); Writing – review & editing (equal). **Dae-Sung Park:** Conceptualization (equal); Project administration (equal); Supervision (equal); Writing – original draft (equal); Writing – review & editing (equal). **Nini Pryds:** Conceptualization (equal); Project administration (equal); Supervision (equal); Writing – original draft (equal); Writing – review & editing (equal).

DATA AVAILABILITY

The data that support the findings of this study are available within the article.

REFERENCES

[1] P. Esquinazi, W. Hergert, D. Spemann, A. Setzer, and A. Ernst, "Defect-induced magnetism in solids," IEEE Trans. Magn. **49**, 4668–4674 (2013).

[2] M. G. Blamire, J. L. MacManus-Driscoll, N. D. Mathur, and Z. H. Barber, "The materials science of functional oxide thin films," Adv. Mater. **21**, 3827–3839 (2009).

[3] L. Schmidt-Mende and J. L. MacManus-Driscoll, "ZnO – nanostructures, defects, and devices," Mater. Today **10**, 40–48 (2007).

[4] K. Yuan *et al.*, "Oxidation induced strain and defects in magnetite crystals," Nat. Commun. **10**, 703 (2019).

[5] A. Herklotz *et al.*, "Strain response of magnetic order in perovskite-type oxide films," Philos. Trans. R. Soc., A **372**, 20120441 (2014).

[6] P. D. Esquinazi *et al.*, "Defect-induced magnetism in nonmagnetic oxides: Basic principles, experimental evidence, and possible devices with ZnO and TiO_2," Phys. Status Solidi B **257**, 1900623 (2020).

[7] W. Li, J. Shi, K. H. L. Zhang, and J. L. MacManus-Driscoll, "Defects in complex oxide thin films for electronics and energy applications: Challenges and opportunities," Mater. Horiz. **7**, 2832–2859 (2020).

[8] A. D. Rata *et al.*, "Defect-induced magnetism in homoepitaxial $SrTiO_3$," APL Mater. **10**, 091108 (2022).

[9] C. Menéndez, D. Chu, and C. Cazorla, "Oxygen-vacancy induced magnetic phase transitions in multiferroic thin films," Npj Comput. Mater. **6**, 76 (2020).

[10] J. B. Goodenough, "An interpretation of the magnetic properties of the perovskite-type mixed crystals $La_{1-x}Sr_xCoO_{3-\lambda}$," J. Phys. Chem. Solids **6**, 287–297 (1958).

[11] A. Chen, Q. Su, H. Han, E. Enriquez, and Q. Jia, "Metal oxide nanocomposites: A perspective from strain, defect, and interface," Adv. Mater. **31**, 1803241 (2019).

[12] D.-S. Park *et al.*, "The emergence of magnetic ordering at complex oxide interfaces tuned by defects," Nat. Commun. **11**, 3650 (2020).

[13] A. M. Oleś, "Magnetic interactions in transition metal oxides with orbital degrees of freedom," AIP Conf. Proc. **695**, 176–187 (2003).

[14] C. Ricca and U. Aschauer, "Mechanisms for point defect-induced functionality in complex perovskite oxides," Appl. Phys. A **128**, 1083 (2022).

[15] A. Pichorim *et al.*, "Theoretical approach to defect-induced magnetism in oxygen-deficient γ-Ga_2O_3 films," Mater. Chem. Phys. **314**, 128877 (2024).

[16] A. Nakamura, K. Matsunaga, J. Tohma, T. Yamamoto, and Y. Ikuhara, "Conducting nanowires in insulating ceramics," Nat. Mater. **2**, 453–456 (2003).

[17] Y. Ikuhara, "Nanowire design by dislocation technology," Prog. Mater. Sci. **54**, 770–791 (2009).

[18] M. D. Armstrong, K.-W. Lan, Y. Guo, and N. H. Perry, "Dislocation-mediated conductivity in oxides: Progress, challenges, and opportunities," ACS Nano **15**, 9211–9221 (2021).

[19] R. Sun, Z. Wang, N. Shibata, and Y. Ikuhara, "A dislocation core in titanium dioxide and its electronic structure," RSC Adv. **5**, 18506–18510 (2015).

[20] J. Wu, F. Long, B. Tang, and X. Tang, "Electronic structure and ferromagnetic properties of Zn vacancies in ZnO screw dislocations: First-principles calculations," AIP Adv. **8**, 065115 (2018).

[21] R. Ishikawa *et al.*, "Room-temperature dilute ferromagnetic dislocations in $Sr_{1-x}Mn_xTiO_{3-\delta}$," Phys. Rev. B **96**, 024440 (2017).

[22] E. A. Volnistem *et al.*, "Controlled dislocation density as enhancer of the magnetic response in multiferroic oxide nanoparticles," Appl. Mater. Today **29**, 101680 (2022).

[23] I. Sugiyama *et al.*, "Ferromagnetic dislocations in antiferromagnetic NiO," Nat. Nanotechnol. **8**, 266–270 (2013).

[24] P. F. Carcia, A. D. Meinhaldt, and A. Suna, "Perpendicular magnetic anisotropy in Pd/Co thin film layered structures," Appl. Phys. Lett. **47**, 178–180 (1985).

[25] A. Ohtomo and H. Y. Hwang, "A high-mobility electron gas at the $LaAlO_3$/$SrTiO_3$ heterointerface," Nature **427**, 423–426 (2004).

[26] Y.-Y. Pai, A. Tylan-Tyler, P. Irvin, and J. Levy, "Physics of $SrTiO_3$ -based heterostructures and nanostructures: A review," Rep. Prog. Phys. **81**, 036503 (2018).

[27] A. Ohtomo and H. Y. Hwang, "Growth mode control of the free carrier density in $SrTiO_{3-\delta}$ films," J. Appl. Phys. **102**, 083704 (2007).

[28] K. A. Müller and H. Burkard, "$SrTiO_3$: An intrinsic quantum paraelectric below 4 K," Phys. Rev. B **19**, 3593–3602 (1979).

[29] R. A. Cowley, "Lattice dynamics and phase transitions of strontium titanate," Phys. Rev. **134**, A981–A997 (1964).

[30] A. Samanta, E. Weinan, and S. B. Zhang, "Method for defect stability diagram from *ab initio* calculations: A case study of $SrTiO_3$," Phys. Rev. B **86**, 195107 (2012).

[31] J. Li *et al.*, "Topotactic phase transformations by concerted dual-ion migration of B-site cation and oxygen in multivalent cobaltite La–Sr.,–Co–O_x films," Nano Energy **78**, 105215 (2020).

[32] C. Lee, J. Destry, and J. L. Brebner, "Optical absorption and transport in semiconducting $SrTiO_3$," Phys. Rev. B **11**, 2299–2310 (1975).

[33] K. Szot, W. Speier, R. Carius, U. Zastrow, and W. Beyer, "Localized metallic conductivity and self-healing during thermal reduction of $SrTiO_3$," Phys. Rev. Lett. **88**, 075508 (2002).

[34] J. M. D. Coey, M. Venkatesan, and P. Stamenov, "Surface magnetism of strontium titanate," J. Phys.: Condens. Matter **28**, 485001 (2016).

[35] A. Lopez-Bezanilla, P. Ganesh, and P. B. Littlewood, "Research update: Plentiful magnetic moments in oxygen deficient $SrTiO_3$," APL Mater. **3**, 100701 (2015).

[36] X. Hao, Z. Wang, M. Schmid, U. Diebold, and C. Franchini, "Coexistence of trapped and free excess electrons in $SrTiO_3$," Phys. Rev. B **91**, 085204 (2015).

[37] D. Park *et al.*, "Electromagnetic functionalization of wide-bandgap dielectric oxides by boron interstitial doping," Adv. Mater. **30**, 1802025 (2018).

[38] L. Zhang *et al.*, "Temperature-independent ferroelectric property and characterization of high- T C m $0.2Bi(Mg_{1/2}Ti_{1/2})O_3$-$0.8PbTiO_3$ thin films," Appl. Phys. Lett. **103**, 082902 (2013).

[39] M. Venkatesan, C. B. Fitzgerald, and J. M. D. Coey, "Unexpected magnetism in a dielectric oxide," Nature **430**, 630–630 (2004).

[40] I. I. Lungu, A. M. Grumezescu, and C. Fleaca, "Unexpected ferromagnetism—A review," Appl. Sci. **11**, 6707 (2021).

[41] X. Jiang *et al.*, "Recent progress on 2D magnets: Fundamental mechanism, structural design and modification," Appl. Phys. Rev. **8**, 031305 (2021).

[42] D. Park *et al.*, "Controlled electronic and magnetic landscape in self-assembled complex oxide heterostructures," Adv. Mater. **35**, 2300200 (2023).

[43] S. Goktas, A. Tumbul, and A. Goktas, "Growth technique–induced highly C-axis-oriented ZnO:Mn, ZnO:Fe and ZnO:Co thin films: A comparison of nanostructure, surface morphology, optical band gap, and room temperature ferromagnetism," J. Supercond. Novel Magn. **36**, 1875–1892 (2023).

[44] J. M. D. Coey, M. Venkatesan, and C. B. Fitzgerald, "Donor impurity band exchange in dilute ferromagnetic oxides," Nat. Mater. **4**, 173–179 (2005).

[45] S. Wang *et al.*, "Titanium-defected undoped anatase TiO_2 with p-type conductivity, room-temperature ferromagnetism, and remarkable photocatalytic performance," J. Am. Chem. Soc. **137**, 2975–2983 (2015).

[46] J. M. D. Coey, "Magnetism in d0 oxides," Nat. Mater. **18**, 652–656 (2019).

[47] Y. F. Wang *et al.*, "Origin of magnetic properties in carbon implanted ZnO nanowires," Sci. Rep. **8**, 7758 (2018).

[48] K. Potzger *et al.*, "Defect-induced ferromagnetism in crystalline $SrTiO_3$," J. Magn. Magn. Mater. **323**, 1551–1562 (2011).

[49] S. Cheng *et al.*, "Manipulation of magnetic properties by oxygen vacancies in multiferroic $YMnO_3$," Adv. Funct. Mater. **26**, 3589–3598 (2016).

[50] P. R. Willmott and J. R. Huber, "Pulsed laser vaporization and deposition," Rev. Mod. Phys. **72**, 315–328 (2000).

[51] J. Shen, Z. Gai, and J. Kirschner, "Growth and magnetism of metallic thin films and multilayers by pulsed-laser deposition," Surf. Sci. Rep. **52**, 163–218 (2004).

[52] G. Z. Liu, Q. Y. Lei, and X. X. Xi, "Stoichiometry of $SrTiO_3$ films grown by pulsed laser deposition," Appl. Phys. Lett. **100**, 202902 (2012).

[53] I. R. Shein and A. L. Ivanovskii, "First principle prediction of vacancy-induced magnetism in non-magnetic perovskite $SrTiO_3$," Phys. Lett. A **371**, 155–159 (2007).

[54] N. Reyren *et al.*, "Superconducting interfaces between insulating oxides," Science **317**, 1196–1199 (2007).

[55] L. Li, C. Richter, J. Mannhart, and R. C. Ashoori, "Coexistence of magnetic order and two-dimensional superconductivity at $LaAlO_3/SrTiO_3$ interfaces," Nat. Phys. **7**, 762–766 (2011).

[56] O. O. Brovko and E. Tosatti, "Controlling the magnetism of oxygen surface vacancies in $SrTiO_3$ through charging," Phys. Rev. Mater. **1**, 044405 (2017).

[57] D. Doennig and R. Pentcheva, "Control of orbital reconstruction in $(LaAlO_3)_M/(SrTiO_3)_N(001)$ quantum wells by strain and confinement," Sci. Rep. **5**, 7909 (2015).

[58] S. D. Yoon *et al.*, "Oxygen-defect-induced magnetism to 880 K in semiconducting anatase $TiO_{2-\delta}$ films," J. Phys.: Condens. Matter **18**, L355–L361 (2006).

[59] M. Salluzzo *et al.*, "Origin of interface magnetism in $BiMnO_3/SrTiO_3$ and $LaAlO_3/SrTiO_3$ heterostructures," Phys. Rev. Lett. **111**, 087204 (2013).

[60] W. A. Adeagbo, G. Fischer, and W. Hergert, "First-principles investigations of electronic and magnetic properties of $SrTiO_3$ (001) surfaces with adsorbed ethanol and acetone molecules," Phys. Rev. B **83**, 195428 (2011).

[61] D. J. Keeble *et al.*, "Identification of A - and B -site cation vacancy defects in perovskite oxide thin films," Phys. Rev. Lett. **105**, 226102 (2010).

[62] H. Hu *et al.*, "Oxygen vacancy dependence of magnetic behavior in the $LaAlO_3/SrTiO_3$ heterostructures," Adv. Mater. Interfaces **3**, 1600547 (2016).

[63] J. Osorio-Guillén, S. Lany, S. V. Barabash, and A. Zunger, "Nonstoichiometry as a source of magnetism in otherwise nonmagnetic oxides: Magnetically interacting cation vacancies and their percolation," Phys. Rev. B **75**, 184421 (2007).

[64] R. W. Ulbricht, A. Schmehl, T. Heeg, J. Schubert, and D. G. Schlom, "Adsorption-controlled growth of EuO by molecular-beam epitaxy," Appl. Phys. Lett. **93**, 102105 (2008).

[65] T. Mairoser *et al.*, "High-quality EuO thin films the easy way via topotactic transformation," Nat. Commun. **6**, 7716 (2015).

[66] H. Jeen *et al.*, "Topotactic phase transformation of the brownmillerite $SrCoO_{2.5}$ to the perovskite $SrCoO_{3\_\delta}$," Adv. Mater. **25**, 3651–3656 (2013).

[67] A. Khare *et al.*, "Topotactic metal–insulator transition in epitaxial $SrFeO_x$ thin films," Adv. Mater. **29**, 1606566 (2017).

[68] D. Li *et al.*, "Emergent and robust ferromagnetic-insulating state in highly strained ferroelastic $LaCoO_3$ thin films," Nat. Commun. **14**, 3638 (2023).

[69] W. S. Choi *et al.*, "Strain-induced spin states in atomically ordered cobaltites," Nano Lett. **12**, 4966–4970 (2012).

[70] J. D. Ferguson *et al.*, "Epitaxial oxygen getter for a brownmillerite phase transformation in manganite films," Adv. Mater. **23**, 1226–1230 (2011).

[71] K. Hu *et al.*, "Atomic-scale observation of strain-dependent reversible topotactic transition in $La_{0.7}Sr_{0.3}MnO_x$ films under an ultra-high vacuum environment," Mater. Today Phys. **29**, 100922 (2022).

[72] E. Ferreiro-Vila, D. Bugallo, C. Magén, F. Rivadulla, and J. M. De Teresa, "Topotactic transformation in $SrFeO_{3-\delta}$ triggered by low-dose Ga + focused ion irradiation," Appl. Phys. Lett. **116**, 163103 (2020).

[73] L. Cao *et al.*, "Migration kinetics of surface ions in oxygen-deficient perovskite during topotactic transitions," Small **17**, 2104356 (2021).

[74] P. Nukala *et al.*, "In situ heating studies on temperature-induced phase transitions in epitaxial $Hf_{0.5}Zr_{0.5}O_2/La_{0.67}Sr_{0.33}MnO_3$ heterostructures," Appl. Phys. Lett. **118**, 062901 (2021).

[75] Y. Wei *et al.*, "A rhombohedral ferroelectric phase in epitaxially strained $Hf_{0.5}Zr_{0.5}O_2$ thin films," Nat. Mater. **17**, 1095–1100 (2018).

[76] P. Puphal *et al.*, "Topotactic transformation of single crystals: From perovskite to infinite-layer nickelates," Sci. Adv. **7**, eabl8091 (2021).

[77] C. Pinta *et al.*, "Suppression of spin-state transition in epitaxially strained $LaCoO_3$," Phys. Rev. B **78**, 174402 (2008).

[78] Z. Yin *et al.*, "Compressive-strain-facilitated fast oxygen migration with reversible topotactic transformation in $La_{0.5}Sr_{0.5}CoO_x$ via all-solid-state electrolyte gating," ACS Nano **16**, 14632–14643 (2022).

[79] M. Merz *et al.*, "X-ray absorption and magnetic circular dichroism of $LaCoO_3$, $La_{0.7}Ce_{0.3}CoO_3$, and $La_{0.7}Sr_{0.3}CoO_3$ films: Evidence for cobalt-valence-dependent magnetism," Phys. Rev. B **82**, 174416 (2010).

[80] S. V. Trukhanov, L. S. Lobanovski, M. V. Bushinsky, I. O. Troyanchuk, and H. Szymczak, "Magnetic phase transitions in the anion-deficient $La_{1-x}Ba_xMnO_{3-x/2}$ $(0 \leq x \leq 0.50)$ manganites," J. Phys. Condens. Matter **15**, 1783–1795 (2003).

[81] H. Huang *et al.*, "Topotactic transition between perovskite and brownmillerite phases for epitaxial $LaCoO_{3-\delta}$ films and effects thus resulted," J. Phys. D: Appl. Phys. **53**, 155003 (2020).

[82] A. K. Mandal *et al.*, "Understanding defect-mediated cubic to hexagonal topotactic phase evolution in $SrMnO_3$ thin films and associated magnetic and electronic properties," Phys. Rev. B **103**, 195110 (2021).

[83] A. Xiao *et al.*, "In-situ investigation on the oxygen vacancy-driven topotactic phase transition in charge-orbital ordered $Nd_{0.5}Sr_{0.5}MnO_3$ films," Acta Mater. **245**, 118616 (2023).

[84] A. Schrön, C. Rödl, and F. Bechstedt, "Crystalline and magnetic anisotropy of the 3d -transition metal monoxides MnO, FeO, CoO, and NiO," Phys. Rev. B **86**, 115134 (2012).

[85] J. Walter *et al.*, "Perpendicular magnetic anisotropy via strain-engineered oxygen vacancy ordering in epitaxial $La_{1-x}Sr_xCoO_{3-\delta}$," Phys. Rev. Mater. **2**, 111404 (2018).

[86] G. Zhou *et al.*, "Overview of magnetic anisotropy evolution in $La_{2/3}Sr_{1/3}MnO_3$-based heterostructures," Sci. China Mater. **66**, 3401–3414 (2023).

[87] D. Yi *et al.*, "Tuning perpendicular magnetic anisotropy by oxygen octahedral rotations in ("$La_{1-x}Sr_xMnO_3$)/($SrIrO_3$) Superlattices," Phys. Rev. Lett. **119**, 077201 (2017).

[88] J. Zhang *et al.*, "Symmetry mismatch-driven perpendicular magnetic anisotropy for perovskite/brownmillerite heterostructures," Nat. Commun. **9**, 1923 (2018).

[89] H. Huang *et al.*, "Tuning magnetic anisotropy by interfacial engineering in $SrFeO_{2.5}/La_{2/3}Ba_{1/3}MnO_3/SrFeO_{2.5}$ trilayers," J. Phys. D: Appl. Phys. **53**, 445001 (2020).

[90] Y. Wang *et al.*, "Robust ferromagnetism in highly strained $SrCoO_3$ thin films," Phys. Rev. X **10**, 021030 (2020).

[91] F. Moussa *et al.*, "Spin waves in the antiferromagnet perovskite $LaMnO_3$: A neutron-scattering study," Phys. Rev. B **54**, 15149–15155 (1996).

[92] J. B. Goodenough, "Theory of the role of covalence in the perovskite-type manganites $[La,M(II)]MnO_3$," Phys. Rev. **100**, 564–573 (1955).

[93] J. Kanamori, "Superexchange interaction and symmetry properties of electron orbitals," J. Phys. Chem. Solids **10**, 87–98 (1959).

[94] N. Lu *et al.*, "Electric-field control of tri-state phase transformation with a selective dual-ion switch," Nature **546**, 124–128 (2017).

[95] Q. Lu *et al.*, "Bi-directional tuning of thermal transport in $SrCoO_x$ with electrochemically induced phase transitions," Nat. Mater. **19**, 655–662 (2020).

[96] C. Leighton, "Electrolyte-based ionic control of functional oxides," Nat. Mater. **18**, 13–18 (2019).

[97] Q. Lu and B. Yildiz, "Voltage-controlled topotactic phase transition in thin-film $SrCoO_x$ monitored by in situ X-ray diffraction," Nano Lett. **16**, 1186–1193 (2016).

[98] Q. Wang *et al.*, "Noble-metal-assisted fast interfacial oxygen migration with topotactic phase transition in perovskite oxides," Adv. Funct. Mater. **31**, 2106765 (2021).

[99] E. Guo *et al.*, "Oxygen diode formed in nickelate heterostructures by chemical potential mismatch," Adv. Mater. **30**, 1705904 (2018).

[100] J. Kitagawa *et al.*, "Interstitial atom engineering in magnetic materials," Metals **10**, 1644 (2020).

[101] T. T. M. Palstra, G. J. Nieuwenhuys, J. A. Mydosh, and K. H. J. Buschow, "Mictomagnetic, ferromagnetic, and antiferromagnetic transitions in La $(Fe_xAl_{1-x})_{13}$ intermetallic compounds," Phys. Rev. B **31**, 4622–4632 (1985).

[102] H. Pan *et al.*, "Room-temperature ferromagnetism in carbon-doped ZnO," Phys. Rev. Lett. **99**, 127201 (2007).

[103] O. I. Malyi, X.-G. Zhao, A. Bussmann-Holder, and A. Zunger, "Local positional and spin symmetry breaking as a source of magnetism and insulation in paramagnetic $EuTiO_3$," Phys. Rev. Mater. **6**, 034604 (2022).

[104] T. Katsufuji and H. Takagi, "Coupling between magnetism and dielectric properties in quantum paraelectric $EuTiO_3$," Phys. Rev. B **64**, 054415 (2001).

[105] K. Tanaka *et al.*, "Ferromagnetism induced by lattice volume expansion and amorphization in $EuTiO_3$ thin films," J. Mater. Res. **28**, 1031–1041 (2013).

[106] C. Li *et al.*, "Strain induced magnetic transitions and spin reorientations in quantum paraelectric $EuTiO_3$ material," J. Magn. Magn. Mater. **382**, 193–201 (2015).

[107] H. Shin *et al.*, "Controlling the electrical and magnetic ground states by doping in the complete phase diagram of titanate $Eu_{1-x}La_xTiO_3$ thin films," Phys. Rev. B **101**, 214105 (2020).

[108] N. Takahara, K. S. Takahashi, Y. Tokura, and M. Kawasaki, "Evolution of ferromagnetism and electron correlation in $Eu_{1-x}Gd_xTiO_3$ thin films with $4f^7$ configuration," Phys. Rev. B **108**, 125138 (2023).

[109] Y. Kususe *et al.*, "Magnetic and transport properties of $EuTiO_3$ thin films doped with Nb," Jpn. J. Appl. Phys. **53**, 05FJ07 (2014).

[110] D. Akahoshi *et al.*, "Magnetic phase diagram for the mixed-valence Eu oxide $EuTi_{1-x}Al_xO_3$ ($0 \leq x \leq 1$)," Phys. Rev. B **96**, 184419 (2017).

[111] W. Zhang *et al.*, "Giant low-field magnetic refrigeration in $EuTi_{1-x}Al_xO_3$ ($x = 0.05$, 0.1 and 0.15) compounds," J. Magn. Magn. Mater. **492**, 165684 (2019).

[112] D. Akahoshi, G. Miyamoto, Y. Hayakawa, and T. Saito, "The magnetic properties of the mixed valence Eu oxide $EuTi_{1\text{-}x}Sc_xO_3$ ($0 \leq x \leq 1$)," J. Solid State Chem. **280**, 120985 (2019).

[113] H. Xie *et al.*, "Investigating the structure, magnetism, magnetocaloric effects and critical behavior of $Eu(Ti,B)O_3$ perovskites," J. Magn. Magn. Mater. **586**, 171185 (2023).

[114] D. Akahoshi, H. Horie, S. Sakai, and T. Saito, "Ferromagnetic behavior mixed valence europium (Eu^{2+}/Eu^{3+}) oxide $EuTi_1\_xMxO_3$ ($M = Al^{3+}$ Ga^{3+})," Appl. Phys. Lett. **103**, 172407 (2013).

[115] D. Shin *et al.*, "Defect engineering of magnetic ground state in $EuTiO_3$ epitaxial thin films," J. Am. Ceram. Soc. **104**, 4606–4613 (2021).

[116] A. Callaghan, C. W. Moeller, and R. Ward, "Magnetic interactions in ternary ruthenium oxides," Inorg. Chem. **5**, 1572–1576 (1966).

[117] S. A. Lee *et al.*, "Tuning electromagnetic properties of $SrRuO_3$ epitaxial thin films via atomic control of cation vacancies," Sci. Rep. **7**, 11583 (2017).

[118] N. S. Garnet *et al.*, "Probing the role of dopant oxidation state in the magnetism of diluted magnetic oxides using Fe-doped In_2O_3 and SnO_2 nanocrystals," J. Phys. Chem. C **121**, 1918–1927 (2017).

[119] X. Wang *et al.*, "Multiferroicity in plastically deformed $SrTiO_3$," Nat. Commun. **15**, 7442 (2024).

[120] M. A. Krivoglaz, V. G. Baryakhtar, M. A. Ivanov, S. C. Moss, and J. Peisl, *X-Ray and Neutron Diffraction in Nonideal Crystals* (Springer, Berlin, Heidelberg, 1996).

[121] L. Sun, D. Marrocchelli, and B. Yildiz, "Edge dislocation slows down oxide ion diffusion in doped CeO_2 by segregation of charged defects," Nat. Commun. **6**, 6294 (2015).

[122] Y. Han *et al.*, "Ultra-dense dislocations stabilized in high entropy oxide ceramics," Nat. Commun. **13**, 2871 (2022).

[123] K. P. McKenna, "Electronic and chemical properties of a surface-terminated screw dislocation in MgO," J. Am. Chem. Soc. **135**, 18859–18865 (2013).

[124] B. Feng *et al.*, "Atomic structures and oxygen dynamics of CeO_2 grain boundaries," Sci. Rep. **6**, 20288 (2016).

[125] K. Ackland and J. M. D. Coey, "Room temperature magnetism in CeO_2 —A review," Phys. Rep. **746**, 1–39 (2018).

[126] N. Shibata *et al.*, "Atomic-scale imaging of individual dopant atoms in a buried interface," Nat. Mater. **8**, 654–658 (2009).

[127] Y. Yan *et al.*, "Impurity-induced structural transformation of a MgO grain boundary," Phys. Rev. Lett. **81**, 3675–3678 (1998).

[128] Z. Wang *et al.*, "Atom-resolved imaging of ordered defect superstructures at individual grain boundaries," Nature **479**, 380–383 (2011).

[129] J. J. Bean and K. P. McKenna, "Stability of point defects near MgO grain boundaries in FeCoB/MgO/FeCoB magnetic tunnel junctions," Phys. Rev. Mater. **2**, 125002 (2018).

[130] Y. Sato, J.-Y. Roh, and Y. Ikuhara, "Grain-boundary structural transformation induced by geometry and chemistry," Phys. Rev. B **87**, 140101 (2013).

[131] B. B. Straumal *et al.*, "Grain boundary layers in nanocrystalline ferromagnetic zinc oxide," JETP Lett. **92**, 396–400 (2010).

[132] M. Coey, K. Ackland, M. Venkatesan, and S. Sen, "Collective magnetic response of CeO_2 nanoparticles," Nat. Phys. **12**, 694–699 (2016).

[133] D. Mishra *et al.*, "Oxygen vacancy enhanced room temperature magnetism in Al-doped MgO nanoparticles," Appl. Phys. Lett. **102**, 182404 (2013).

[134] J. M. D. Coey, J. T. Mlack, M. Venkatesan, and P. Stamenov, "Magnetization process in dilute magnetic oxides," IEEE Trans. Magn. **46**, 2501–2503 (2010).

[135] S. S. Farvid *et al.*, "Evidence of charge-transfer ferromagnetism in transparent diluted magnetic oxide nanocrystals: Switching the mechanism of magnetic interactions," J. Am. Chem. Soc. **136**, 7669–7679 (2014).

[136] H. Vahidi *et al.*, "A review of grain boundary and heterointerface characterization in polycrystalline oxides by (scanning) transmission electron microscopy," Crystals **11**, 878 (2021).

[137] W. Amin, M. Ali, N. Vajragupta, and A. Hartmaier, "Studying grain boundary strengthening by dislocation-based strain gradient crystal plasticity coupled with a multi-phase-field model," Materials **12**, 2977 (2019).

[138] S. Ikeda *et al.*, "A perpendicular-anisotropy CoFeB–MgO magnetic tunnel junction," Nat. Mater. **9**, 721–724 (2010).

[139] G. Yu *et al.*, "Switching of perpendicular magnetization by spin–orbit torques in the absence of external magnetic fields," Nat. Nanotechnol. **9**, 548–554 (2014).

[140] A. Chen *et al.*, "Tunable low-field magnetoresistance in $(La_{0.7}Sr_{0.3}MnO_3)_{0.5}$:$(ZnO)_{0.5}$ self-assembled vertically aligned nanocomposite thin films," Adv. Funct. Mater. **21**, 2423–2429 (2011).

[141] S.-C. Liao *et al.*, "Misorientation control and functionality design of nanopillars in self-assembled perovskite−spinel heteroepitaxial nanostructures," ACS Nano **5**, 4118–4122 (2011).

[142] N. Dix *et al.*, "Selectable spontaneous polarization direction and magnetic anisotropy in $BiFeO_3$ $-CoFe_2O_4$ epitaxial nanostructures," ACS Nano **4**, 4955–4961 (2010).

[143] N. M. Aimon, D. Hun Kim, H. Kyoon Choi, and C. A. Ross, "Deposition of epitaxial $BiFeO_3/CoFe_2O_4$ nanocomposites on (001) $SrTiO_3$ by combinatorial pulsed laser deposition," Appl. Phys. Lett. **100**, 092901 (2012).

[144] S. Cho *et al.*, "Self-assembled oxide films with tailored nanoscale ionic and electronic channels for controlled resistive switching," Nat. Commun. **7**, 12373 (2016).

[145] S. Petzold *et al.*, "Forming-free grain boundary engineered hafnium oxide resistive random access memory devices," Adv. Electron. Mater. **5**, 1900484 (2019).

[146] J. J. Bean *et al.*, "Atomic structure and electronic properties of MgO grain boundaries in tunnelling magnetoresistive devices," Sci. Rep. **7**, 45594 (2017).

[147] A. Banerjee, K. V. L. V. Narayanachari, and S. Raghavan, "Effect of in situ stress on grain growth and texture evolution in sputtered YSZ/Si films," RSC Adv. **7**, 17832–17840 (2017).

[148] Y. Zhang and W. J. Weber, "Ion irradiation and modification: The role of coupled electronic and nuclear energy dissipation and subsequent nonequilibrium processes in materials," Appl. Phys. Rev. **7**, 041307 (2020).

[149] J. F. Ziegler, M. D. Ziegler, and J. P. Biersack, "SRIM – The stopping and range of ions in matter (2010)," Nucl. Instrum. Methods Phys. Res., B **268**, 1818–1823 (2010).

[150] S. Zhou *et al.*, "Origin of magnetic moments in defective TiO_2 single crystals," Phys. Rev. B **79**, 113201 (2009).

[151] H. Thakur *et al.*, "Irradiation induced ferromagnetism at room temperature in TiO_2 thin films: X-ray magnetic circular dichroism characterizations," Appl. Phys. Lett. **98**, 192512 (2011).

[152] D. Sanyal *et al.*, "Room temperature ferromagnetic ordering in 4 MeV Ar^{5+} irradiated TiO_2," J. Phys. D: Appl. Phys. **47**, 025001 (2014).

[153] M. Stiller *et al.*, "Titanium 3 D ferromagnetism with perpendicular anisotropy in defective anatase," Phys. Rev. B **101**, 014412 (2020).

[154] M. Stiller and P. D. Esquinazi, "Defect-induced magnetism in TiO_2: An example of quasi 2D magnetic order with perpendicular anisotropy," Front. Phys. **11**, 1124924 (2023).

[155] S. Zhou *et al.*, "Ferromagnetism and suppression of metallic clusters in Fe implanted ZnO: A phenomenon related to defects?," J. Phys. D: Appl. Phys. **41**, 105011 (2008).

[156] B. Panigrahy, M. Aslam, and D. Bahadur, "Controlled optical and magnetic properties of ZnO nanorods by Ar ion irradiation," Appl. Phys. Lett. **98**, 183109 (2011).

[157] S. Mal, S. Nori, J. Narayan, J. T. Prater, and D. K. Avasthi, "Ion-irradiation-induced ferromagnetism in undoped ZnO thin films," Acta Mater. **61**, 2763–2768 (2013).

[158] P. Satyarthi *et al.*, "Defect controlled ferromagnetism in xenon ion irradiated zinc oxide," J. Magn. Magn. Mater. **385**, 318–325 (2015).

[159] I. Lorite *et al.*, "Advances in methods to obtain and characterise room temperature magnetic ZnO," Appl. Phys. Lett. **106**, 082406 (2015).

[160] V. Fernandes *et al.*, "Ferromagnetism induced by oxygen and cerium vacancies above the percolation limit in CeO_2," J. Phys.: Condens. Matter **22**, 216004 (2010).

[161] K. Shimizu *et al.*, "Change in magnetic properties induced by swift heavy ion irradiation in CeO_2," Nucl. Instrum. Methods Phys. Res., B **286**, 291–294 (2012).

[162] A. Singh, R. Saini, P. Kumar, and A. Kandasami, “Tailoring of defects dependent magnetic properties of swift heavy ion irradiated CeO_2 for spintronics application,” J. Appl. Phys. **132**, 125901 (2022).

[163] Lorite, I. *et al.* “Study of the negative magneto-resistance of single proton-implanted lithium-doped ZnO microwires,” J. Phys. Condens. Matter **27**, 256002 (2015).

[164] Dietl, T., Bonanni, A., and Ohno, H, “Families of magnetic semiconductors — An overview,” J. Semicond. **40**, 080301 (2019).

[165] M. Friák *et al.*, “Vacancy-induced magnetic states in TiO_2 surfaces,” J. Appl. Phys. **134**, 013902 (2023).

[166] C. Wang *et al.*, “Topological hall effect in single thick $SrRuO_3$ layers induced by defect engineering,” Adv. Electron. Mater. **6**, 2000184 (2020).

[167] H. Guo *et al.*, “Strain doping: Reversible single-axis control of a complex oxide lattice via helium implantation,” Phys. Rev. Lett. **114**, 256801 (2015).

[168] E. O. Wollan and W. C. Koehler, “Neutron diffraction study of the magnetic properties of the series of perovskite-type compounds [(1−x)La,xCa] MnO_3,” Phys. Rev. **100**, 545–563 (1955).

[169] J. Rodríguez-Carvajal *et al.*, “Neutron-diffraction study of the Jahn-Teller transition in stoichiometric $LaMnO_3$,” Phys. Rev. B **57**, R3189–R3192 (1998).

[170] H. Yamada, P.-H. Xiang, and A. Sawa, “Phase evolution and critical behavior in strain-tuned $LaMnO_3$-$SrMnO_3$ superlattices,” Phys. Rev. B **81**, 014410 (2010).

[171] H. Yamada, M. Kawasaki, T. Lottermoser, T. Arima, and Y. Tokura, “$LaMnO_3$/$SrMnO_3$ interfaces with coupled charge-spin-orbital modulation,” Appl. Phys. Lett. **89**, 052506 (2006).

[172] B. R. K. Nanda and S. Satpathy, “Effects of strain on orbital ordering and magnetism at perovskite oxide interfaces: $LaMnO_3$/$SrMnO_3$,” Phys. Rev. B **78**, 054427 (2008).

[173] B. R. K. Nanda and S. Satpathy, “Magnetic and orbital order in $LaMnO_3$ under uniaxial strain: A model study,” Phys. Rev. B **81**, 174423 (2010).

[174] J. Garcia-Barriocanal *et al.*, “Spin and orbital Ti magnetism at $LaMnO_3$/$SrTiO_3$ interfaces,” Nat. Commun. **1**, 82 (2010).

[175] X. R. Wang *et al.*, “Imaging and control of ferromagnetism in $LaMnO_3$/$SrTiO_3$ heterostructures,” Science **349**, 716–719 (2015).

[176] Z. Chen *et al.*, “Electron accumulation and emergent magnetism in $LaMnO_3$/$SrTiO_3$ heterostructures,” Phys. Rev. Lett. **119**, 156801 (2017).

[177] M. J. R. Hoch *et al.*, “Diamagnetic to paramagnetic transition in $LaCoO_3$,” Phys. Rev. B **79**, 214421 (2009).

[178] D. Fuchs *et al.*, “Ferromagnetic order in epitaxially strained $LaCoO_3$ thin films,” Phys. Rev. B **75**, 144402 (2007).

[179] D. Fuchs *et al.*, “Tuning the magnetic properties of $LaCoO_3$ thin films by epitaxial strain,” Phys. Rev. B **77**, 014434 (2008).

[180] V. V. Mehta *et al.*, “Ferromagnetism in tetragonally distorted $LaCoO_3$ thin films,” J. Appl. Phys. **105**, 07E503 (2009).

[181] D. Shin *et al.*, “Tunable ferromagnetism in $LaCoO_3$ epitaxial thin films,” Adv. Mater. Interfaces **9**, 2200433 (2022).

[182] N. Biškup *et al.*, “Insulating ferromagnetic $LaCoO_{3-\delta}$ films: A phase induced by ordering of oxygen vacancies,” Phys. Rev. Lett. **112**, 087202 (2014).

[183] N. Zhang *et al.*, “Oxygen vacancy ordering modulation of magnetic anisotropy in strained $LaCoO_{3-x}$ thin films,” ACS Appl. Mater. Interfaces **10**, 38230–38238 (2018).

[184] S. Park *et al.*, “Microscopic evidence of a strain-enhanced ferromagnetic state in $LaCoO_3$ thin films,” Appl. Phys. Lett. **95**, 072508 (2009).

[185] A. M. Durand *et al.*, “The effects of Co_3O_4 on the structure and unusual magnetism of $LaCoO_3$,” J. Phys.: Condens. Matter **27**, 126001 (2015).

[186] Y. Lin *et al.*, “Vertical strain-driven antiferromagnetic to ferromagnetic phase transition in $EuTiO_3$ nanocomposite thin films,” ACS Appl. Mater. Interfaces **12**, 8513–8521 (2020).

[187] A. Chen *et al.*, “Role of scaffold network in controlling strain and functionalities of nanocomposite films,” Sci. Adv. **2**, e1600245 (2016).

[188] L. M. C. Pereira, “Experimentally evaluating the origin of dilute magnetism in nanomaterials,” J. Phys. D: Appl. Phys. **50**, 393002 (2017).

[189] D. V. Christensen *et al.*, “2024 roadmap on magnetic microscopy techniques and their applications in materials science,” J. Phys. Mater. **7**, 032501 (2024).

[190] D. Hurt, S. Li, and A. Amann, “Versatile SQUID susceptometer with multiple measurement modes,” IEEE Trans. Magn. **49**, 3541–3544 (2013).

[191] J. M. D. Coey and S. S. P. Parkin, *Handbook of Magnetism and Magnetic Materials* (Springer International Publishing, Cham, 2021).

[192] G. Van Der Laan and A. I. Figueroa, “X-ray magnetic circular dichroism—A versatile tool to study magnetism,” Coord. Chem. Rev. **277–278**, 95–129 (2014).

[193] G. Malsch *et al.*, “Correlating the nanoscale structural, magnetic, and magneto-transport properties in $SrRuO_3$ -based perovskite thin films: implications for oxide skyrmion devices,” ACS Appl. Nano Mater. **3**, 1182–1190 (2020).

[194] S. Mühlbauer *et al.*, “Magnetic small-angle neutron scattering,” Rev. Mod. Phys. **91**, 015004 (2019).

[195] E.-J. Guo *et al.*, “Nanoscale ferroelastic twins formed in strained $LaCoO_3$ films,” Sci. Adv. **5**, eaav5050 (2019).

[196] E. Cancès and G. Friesecke, *Density Functional Theory: Modeling, Mathematical Analysis, Computational Methods, and Applications* (Springer International Publishing, Cham, 2023).

[197] F. Calavalle *et al.*, “Gate-tuneable and chirality-dependent charge-to-spin conversion in tellurium nanowires,” Nat. Mater. **21**, 526–532 (2022).

[198] I. V. Maznichenko, P. Buczek, I. Mertig, and S. Ostanin, “Spin textures induced in n-doped solid electrolytes,” J. Phys. D: Appl. Phys. **56**, 405305 (2023).

[199] Y. A. Bychkov and E. I. Rashba, “Oscillatory effects and the magnetic susceptibility of carriers in inversion layers,” J. Phys. C: Solid State Phys. **17**, 6039–6045 (1984).

[200] Y. Matsumoto *et al.*, “Ferromagnetism in Co-doped TiO_2 rutile thin films grown by laser molecular beam epitaxy,” Jpn. J. Appl. Phys. **40**, L1204 (2001).

[201] Y. H. Chang *et al.*, “Observation of room temperature ferromagnetic behavior in cluster-free, Co doped HfO_2 films,” Appl. Phys. Lett. **91**, 082504 (2007).

[202] P. Kharel *et al.*, “Room temperature ferromagnetism in Cr-doped In_2O_3 on high vacuum annealing of thin films and bulk samples,” J. Appl. Phys. **101**, 09H117 (2007).

[203] T. Dietl, H. Ohno, F. Matsukura, J. Cibert, and D. Ferrand, “Zener model description of ferromagnetism in zinc-blende magnetic semiconductors,” Science **287**, 1019–1022 (2000).

[204] S. Ostanin *et al.*, “Mn-stabilized zirconia: From imitation diamonds to a new potential high- T_C ferromagnetic spintronics material,” Phys. Rev. Lett. **98**, 016101 (2007).

[205] S. Gariglio, N. Reyren, A. D. Caviglia, and J.-M. Triscone, “Superconductivity at the $LaAlO_3$/$SrTiO_3$ interface,” J. Phys.: Condens. Matter **21**, 164213 (2009).

[206] Y. Gan, Y. Zhang, D. V. Christensen, N. Pryds, and Y. Chen, “Gate-tunable Rashba spin-orbit coupling and spin polarization at diluted oxide interfaces,” Phys. Rev. B **100**, 125134 (2019).

[207] A. Brinkman *et al.*, “Magnetic effects at the interface between non-magnetic oxides,” Nat. Mater. **6**, 493–496 (2007).

[208] J. A. Bert *et al.*, “Direct imaging of the coexistence of ferromagnetism and superconductivity at the $LaAlO_3$/$SrTiO_3$ interface,” Nat. Phys. **7**, 767–771 (2011).

[209] B. Kalisky *et al.*, “Critical thickness for ferromagnetism in $LaAlO_3$/$SrTiO_3$ heterostructures,” Nat. Commun. **3**, 922 (2012).

[210] S. Sen, K. S. Gupta, and J. M. D. Coey, “Mesoscopic structure formation in condensed matter due to vacuum fluctuations,” Phys. Rev. B **92**, 155115 (2015).

[211] R. Pentcheva and W. E. Pickett, “Avoiding the polarization catastrophe in $LaAlO_3$ overlayers on $SrTiO_3$(001) through polar distortion,” Phys. Rev. Lett. **102**, 107602 (2009).

[212] A. I. Liechtenstein, V. I. Anisimov, and J. Zaanen, “Density-functional theory and strong interactions: Orbital ordering in Mott-Hubbard insulators,” Phys. Rev. B **52**, R5467–R5470 (1995).

[213] H. Banerjee, S. Banerjee, M. Randeria, and T. Saha-Dasgupta, “Electronic structure of oxide interfaces: A comparative analysis of $GdTiO_3$/$SrTiO_3$ and $LaAlO_3$/$SrTiO_3$ interfaces,” Sci. Rep. **5**, 18647 (2015).

[214] K. J. Kormondy *et al.*, “Large positive linear magnetoresistance in the two-dimensional t_{2g} electron gas at the EuO/$SrTiO_3$ interface,” Sci. Rep. **8**, 7721 (2018).

[215] R. Di Capua *et al.*, "Orbital selective switching of ferromagnetism in an oxide quasi two-dimensional electron gas," Npj Quantum Mater. **7**, 41 (2022).

[216] I. V. Maznichenko *et al.*, "Emerging two-dimensional conductivity at the interface between mott and band insulators," Phys. Rev. Lett. **132**(21), 216201 (2024).

[217] I. V. Maznichenko, S. Ostanin, I. Mertig, and P. Buczek, "Emergent quasi-two-dimensional electron gas between $Li_{1\pm x}NbO_3$ and $LaAlO_3$ and its prospectively switchable magnetism," Phys. Rev. Mater. **5**, 114001 (2021).

[218] I. V. Maznichenko, P. Buczek, I. Mertig, and S. Ostanin, "Charge-to-spin conversion in the quasi-two-dimensional electron gas emerging at the hydrogen-doped interface between $LiNbO_3$ and $LaAlO_3$," Phys. Rev. Mater. **6**, 064001 (2022).

[219] N. Mott, *Metal-Insulator Transitions* (CRC Press, 2004).

[220] M. Mochizuki and M. Imada, "Orbital physics in the perovskite Ti oxides," New J. Phys. **6**, 154 (2004).

[221] J. M. Rondinelli, S. J. May, and J. W. Freeland, "Control of octahedral connectivity in perovskite oxide heterostructures: An emerging route to multifunctional materials discovery," MRS Bull. **37**, 261–270 (2012).

[222] J. M. Rondinelli and N. A. Spaldin, "Substrate coherency driven octahedral rotations in perovskite oxide films," Phys. Rev. B **82**, 113402 (2010).

[223] H. W. Yang *et al.*, "Anomalous magnetism in strained $La_{1-x}Sr_xCoO_3$ epitaxial films ($0 \le x \le 0.5$)," Sci. Rep. **4**, 6206 (2014).

[224] D. Fuchs *et al.*, "Double exchange via t_{2g} orbitals and the Jahn-Teller effect in ferromagnetic $La_{0.7}Sr_{0.3}CoO_3$ probed by epitaxial strain," Phys. Rev. Lett. **111**, 257203 (2013).

[225] J. M. Rondinelli and N. A. Spaldin, "Structure and properties of functional oxide thin films: Insights from electronic-structure calculations," Adv. Mater. **23**, 3363–3381 (2011).

[226] H. Han *et al.*, "Control of oxygen vacancy ordering in brownmillerite thin films via ionic liquid gating," ACS Nano **16**, 6206–6214 (2022).